The non-statistical dynamics of the $^{18}O + {}^{32}O_2$ isotope exchange reaction at two energies

Annalise L. Van Wyngarden,[1,a)] Kathleen A. Mar,[2,b)] Jim Quach,[3] Anh P. Q. Nguyen,[3] Aaron A. Wiegel,[2] Shi-Ying Lin,[4,5] Gyorgy Lendvay, [6] Hua Guo,[4] Jim J. Lin,[7,8] Yuan T. Lee,[7,8] and Kristie A. Boering[2,9]

[1]*Department of Chemistry, San José State University, San Jose, CA 95192, USA*

[2]*Department of Chemistry, University of California, Berkeley, CA 94720, USA*

[3]*Department of Mathematics, San José State University, San Jose, CA 95192, USA*

[4]*Department of Chemistry and Chemical Biology, University of New Mexico, Albuquerque, NM 87131, USA*

[5]*School of Physics, Shandong University, Jinan 250100, China*

[6]*Institute for Materials and Environmental Chemistry, Research Centre for Natural Sciences, Hungarian Academy of Sciences, P.O.B. 286, Budapest, H-1519, Hungary*

[7]*Institute of Atomic and Molecular Sciences, Academia Sinica, Taipei, 10617, Taiwan*

[8]*Department of Chemistry, National Taiwan University, Taipei 10617, Taiwan*

[9]*Department of Earth and Planetary Science, University of California, Berkeley, CA 94720, USA*

[a)]*Author to whom correspondence should be addressed. Electronic mail: Annalise.VanWyngarden@sjsu.edu*

[b)]*Present address: Institute for Advanced Sustainability Studies, Potsdam D-14467, Germany*

Abstract

The dynamics of the $^{18}O(^3P) + {}^{32}O_2$ isotope exchange reaction were studied using crossed atomic and molecular beams at collision energies (E_{coll}) of 5.7 and 7.3 kcal/mol, and experimental results were compared with quantum statistical (QS) and quasi-classical trajectory (QCT) calculations on the $O_3(X^1A')$ potential energy surface (PES) of Babikov *et al*. [D. Babikov, B. K. Kendrick, R. B. Walker, R. T. Pack, P. Fleurat-Lesard, and R. Schinke, J. Chem. Phys. **118**, 6298 (2003)]. In both QS and QCT calculations, agreement with experiment was markedly improved by performing calculations with the experimental distribution of collision energies instead of fixed at the average collision energy. At both collision energies, the scattering displayed a forward bias, with a smaller bias at the lower E_{coll}. Comparisons with the QS calculations suggest that $^{34}O_2$ is produced with a non-statistical rovibrational distribution that is hotter than predicted, and the discrepancy is larger at the lower E_{coll}. If this underprediction of rovibrational excitation by the QS method is not due to PES errors and/or to non-adiabatic effects not included in the calculations, then this collision energy dependence is opposite to what might be expected based on collision complex lifetime arguments and opposite to that measured for the forward bias. While the QCT calculations captured the experimental product vibrational energy distribution better than the QS method, the QCT results underpredicted rotationally-excited products, overpredicted forward-bias and predicted a trend in the strength of forward-bias with collision energy opposite to that measured, indicating that it does not completely capture the dynamic behavior measured in the experiment. Thus, these results further underscore the need for improvement in theoretical treatments of dynamics on the $O_3(X^1A')$ PES and perhaps of the PES itself in order to better understand and predict non-statistical effects in this reaction and in the

formation of ozone (in which the intermediate O_3* complex is collisionally stabilized by a third body). The scattering data presented here at two different collision energies provide important benchmarks to guide these improvements.

I. INTRODUCTION

The O + O_2 oxygen atom exchange reaction (R1) occurs on the same potential energy surface (PES) as ozone formation (R2) and, like ozone formation, shows unusually large kinetic isotope effects that cannot be explained by statistical reaction rate theories.[1,2,3,4,5]

$$O(^3P) + O_2 \rightarrow O_3^* \rightarrow O_2 + O(^3P) \quad \text{(R1)}$$

$$O(^3P) + O_2 + M \rightarrow O_3^* + M \rightarrow O_3 + M^* \quad \text{(R2)}$$

The failure of statistical theories[6] and the facts that theoretical treatments require *ad hoc* limits on the lifetimes of O_3* or bottlenecks in intermolecular energy transfer that are larger for the symmetric versus asymmetric isotopologs of O_3* (e.g., $^{16}O^{16}O^{16}O$ vs $^{18}O^{16}O^{16}O$) (e.g., Refs 5, 7, 8, 9, 10, 11, 12) or implicate differences in tunneling lifetimes due to distortions in the vibrational wavefunctions for asymmetric O_3*,[(13)] all indicate that dynamics must play a role in (R1), (R2), or both. Until recently, however, the dynamics of (R1) had not been measured directly by experiment.

Reaction (R1) is a complex-forming reaction with a barrierless reaction pathway. In the statistical limit, the lifetime of the reaction intermediate in a complex-forming reaction is sufficiently long that the energy is completely randomized among all degrees of freedom, resulting in a forward-backward symmetric angular distribution for the products.[14] Reactive scattering experiments for (R3) at a collision energy (E_{coll}) of 7.3 kcal/mol[15] provided the first direct experimental evidence for non-statistical behavior in the decomposition of excited ozone complexes:

$$^{18}O(^3P) + {}^{32}O_2(^3\Sigma_g^-) \rightarrow {}^{50}O_3^* \rightarrow {}^{16}O(^3P) + {}^{34}O_2(^3\Sigma_g^-) \qquad \text{(R3)}$$

The experiment showed a pronounced forward bias in reactive scattering, indicating an O_3* complex that is short-lived with respect to its rotational period and, hence, one in which intramolecular vibrational energy redistribution (IVR) is likely incomplete before dissociation occurs. Comparisons with quantum statistical (QS)[16] calculations suggested that the rovibrational energy distribution in the product $^{34}O_2$ was also non-statistical, at least if it is assumed that the PES used in the calculations is accurate and non-adiabatic effects are not important.[15] Comparisons with reaction dynamics calculations using the quasi-classical trajectory (QCT) method corroborated that non-statistical effects characterize the reaction (R1).[15]

In order to gain additional insight into the non-statistical behavior in the dynamics of the O + O_2 isotope exchange reaction measured at 7.3 kcal/mol, experiments at a lower collision energy of 5.7 kcal/mol were performed and are presented here and compared to the E_{coll} = 7.3 kcal/mol results and to QS and QCT calculations. Notably, to ensure the robustness of conclusions based on experiment/theory comparisons, we have explicitly addressed the possibility that discrepancies between experiment and theory could be due in part to performing theoretical calculations with E_{coll} fixed at the average experimental collision energy while the experiments represent results for a distribution of E_{coll}. This new analysis illustrates that performing theoretical calculations with an experimental distribution of E_{coll} can improve agreement with experiment, while the expansion of the crossed-beam scattering experiments to more than one collision energy provides a more rigorous test for theories used to treat the O + O_2 isotope exchange and ozone formation reactions and the potential energy surfaces (PESs) involved[17] as well as for theories that treat barrierless, deep potential well reactions in general.

II. EXPERIMENTAL AND THEORETICAL METHODS

Crossed beam experiments were performed for the $^{18}O(^3P) + {}^{32}O_2 \rightarrow {}^{16}O(^3P) + {}^{34}O_2$ reaction using the universal crossed beam apparatus[18,19] shown schematically in Fig. 1, and included production of a 50:50 beam of $O(^3P)$ and $O(^1D)$ from photolysis of $^{36}O_2$ (< 0.1% ^{16}O) at 157.6 nm by a F_2 excimer laser (Lambda Physik, LPX 210i, 50Hz.). Experimental details and conditions were the same as those described in Van Wyngarden *et al.*[15] except that the collision energy (E_{coll}) was decreased from 7.3 kcal/mol to 5.7 kcal/mol by decreasing the velocity of the reactant ^{18}O beam. This reduction was accomplished by modifying the orientation of the pulsed valve for the photolytic precursor $^{36}O_2$ since the Lab-frame velocity of the resulting O-atom is a vector sum of the precursor O_2 velocity and the recoil velocity from photolysis. To get the faster O-atom beam of speed 2170 m/s, the O_2 beam was about 70 degrees (upwards) away from the scattering plane (the horizontal plane); the slower O-atom beam (1887 m/s) was obtained by rotating the O_2 beam to 90 degrees away from the scattering plane, which was the maximum angle attainable, limited by the source chamber geometry.

The only significant difference in the modified ("slow") ^{18}O atomic beam from the "fast" ^{18}O atomic beam was the slower average velocity of 1887 m/s (compared to 2170 m/s). The speed ratios for the slow and fast ^{18}O beams were not significantly different (25 and 28, respectively), however, and the angular divergences were identical (± 4.5° FWHM). The $^{32}O_2$ molecular beams were essentially identical for the experiments at both collision energies, with average velocities of 784 m/s and 783 m/s and angular divergences of ±1.6° and ±1.7° FWHM for E_{coll} = 5.7 and 7.3 kcal/mol, respectively, and identical speed ratios of 18. (Uncertainties in the absolute velocities are ~1-2%.) Crossing the ^{18}O atomic beam with the $^{32}O_2$ molecular beam at 90° resulted in average collision energies of 5.7 ± 0.35 kcal/mol and 7.3 ± 0.41 kcal/mol (±1σ)

for the slow and fast ^{18}O beams, respectively (see below for discussion of the method for calculating E_{coll} widths).

Time-of-flight (TOF) spectra for the isotope exchange product $^{34}O_2$ in the E_{coll} = 5.7 kcal/mol experiments were collected at 5 different laboratory angles between 20° and 55° (with the O atom beam defined as 0°), while those for the E_{coll} = 7.3 kcal/mol experiments were collected between 10° and 60°. The smaller range for the 5.7 kcal/mol experiments was selected to best cover the center-of-mass (COM) angular range of scattering for the v = 1 channel of the product $^{34}O_2$ only since the large background in the v = 0 backward scattering region prohibited sampling that would be sufficient to distinguish differences in the angular distribution of the v = 0 channel from that in the 7.3 kcal/mol experiments (which also showed a large uncertainty in the backward scattering region). Newton diagrams (Figures 2 and 3) demonstrate that at both collision energies the backward scattering region for v = 0 was close to the $^{32}O_2$ beam at 90°. Therefore, the peak of the backward scattering region was experimentally inaccessible since the large background from natural abundance $^{34}O_2$ (0.4%) in the unlabeled O_2 beam overwhelmed the signal at angles greater than 60°. We note, however, that the 7.3 kcal/mol experiments were not fully blind to backward scattering from the v = 0 channel since the v = 0 TOF peak had significant width that extended all the way to the v = 1 peak (see Van Wyngarden *et al.*[15]). Since the uncertainties in the backward scattering region prohibited the detection of differences between the v = 0 angular distributions at 7.3 and 5.7 kcal/mol, the angular range for the 5.7 kcal/mol experiment was chosen to sample only those angles necessary to cover the entire COM angular distribution of the v = 1 channel, while at the same time also sampling the v = 0 channel at sideways scattering angles, thus still providing the product translational energy distribution for the v = 0 channel.

After TOF spectra were collected at the angles noted above, the raw TOF spectra were corrected for background $^{34}O_2$ that undergoes inelastic scattering with the O atomic beam by measuring the large $^{32}O_2$ inelastic scattering signal at each angle, scaling to the natural abundance of $^{34}O_2$, and then subtracting this scaled background from the raw $^{34}O_2$ TOF spectra, as described previously.[15] At 5.7 kcal/mol, the correction ranged from 10% of the v = 0 peak height at 20° to 43% at 55°, while at 7.3 kcal/mol the correction ranged from 6% of the v = 0 peak height at 10° to 48% at 60°. After this background correction and rebinning the data to 3μs to improve the signal-to-noise ratio, the resulting TOF spectra were fit empirically using an iterative forward convolution method that accounts for machine parameters, beam characteristics, and the center-of-mass to lab frame conversion, as described previously.[15,18,19] Two channels with separate angular and translational energy distributions (i.e., $P(\theta)$ and $P(E_t)$, respectively) for $^{34}O_2$ in the v = 0 and v = 1 states were included in the fits.

We note that, due to both experimental scatter in the TOF data and overlap of the v = 0 and v = 1 channels (particularly for E_{coll} = 7.3 kcal/mol), there are ranges of values for the $P(\theta)$s, $P(E_t)$s, and the v = 1 branching ratios that can be combined in various ways to produce at least adequate simulations of the data. We have attempted to conservatively estimate these uncertainties for the 7.3 kcal/mol data by giving a range of parameter values that are consistent with the experimental TOF data. These ranges for $P(\theta)$ and $P(E_t)$ are shown by gray shaded areas in several of the figures below, while the range of adequate v = 1 branching ratios was 7-30%. Note that the shaded regions greatly overestimate the uncertainty, however, since the $P(\theta)$s, $P(E_t)$s, and branching ratios cannot be varied independently. Nevertheless, they provide some useful insight in comparisons of the experiments at the different collision energies to each other and to theoretical predictions by demonstrating where uncertainties are largest.

The $^{18}O + {}^{32}O_2$ isotope exchange reaction was also simulated using the QS and QCT theoretical methods at both collision energies. The QS calculations were performed as described in Van Wyngarden *et al.*[15] for comparisons with the E_{coll} = 7.3 kcal/mol experiments. The QS model treats reactive scattering on a statistical basis, assuming that the reaction intermediate is long-lived.[20,21,22] For example, the state-to-state reaction probability is given by $P_{f\leftarrow i} = p_i^{(c)} p_f^{(c)} / \Sigma_l p_l^{(c)}$, where the $p_i^{(c)}$ and $p_f^{(c)}$ are the quantum capture probabilities for the reactant (*i*) and product (*f*) channels, respectively, and the sum is over all open channels. The differential cross sections were calculated using a random phase approximation, which implies a forward-backward symmetry in the angular distribution. Importantly, the quantum treatment of the capture processes allows an accurate description of quantum effects such as tunneling and zero-point energies. By design, however, the QS model cannot describe short time scale events but does serve as a useful limiting case for long-lived complex-forming reactions. The QCT calculations were based on Newtonian mechanics with quantized initial conditions. The calculations were performed as described in Van Wyngarden *et al.*,[15] except that the current calculations employed an improved Gaussian-weighting technique to impose quantization of the product vibrational state by weighting trajectories higher when they result in classical vibrational quantum numbers closer to an integer (0 and 1 in our case).[23] The width of the Gaussian window has been set to 0.05 (in vibrational quantum number).[24] Note that increasing the width parameter to 0.25 washes out the v = 1 peak of the $P(E_t)$ (see below). The conventional QCT histogram method is not able to predict the separate v = 1 peak either. At each collision energy, 4 million trajectories were integrated. While the QCT approach can account for the full dynamics, its treatment of the zero-point energy and other quantum features such as resonances is often

unsatisfactory. Both the QS and QCT methods employed the $O_3(X^1A')$ PES of Babikov *et al.*[17] as in our earlier work.[15]

The conventional way of comparing theoretical and experimental TOF spectra is that the calculations are performed at fixed collision energies (E_{coll} = 5.7 and 7.3 kcal/mol in the present case), and the $P(\theta)$s and $P(E_t)$s predicted by the QS and QCT methods are then used to simulate the laboratory-frame TOF data. $P(E_t)$s for comparison with experiment are calculated from the theoretical rovibrational populations using the Gaussian convolution method[25] to account for the fact that collisions in the experiment occur with a distribution of initial translational energies. The $P(\theta)$ and $P(E_t)$ distributions predicted by these fixed collision energy QS and QCT calculations, with $P(E_t)$s dispersed this way, were used to simulate the laboratory-frame TOF data for comparison with experimental results, along with direct comparisons of the distributions with those derived empirically from the experimental TOF data.

The method described above for predicting TOF data from QS and QCT calculations (performed at fixed collision energies) takes into account the effect of the width of the experimental collision energy distributions on the product $P(E_t)$s in an *ad hoc* manner via the Gaussian convolution method. This method disperses the translational energy distributions, $P(E_t)$s, derived from the rovibrational state distributions using the width of the experimental E_{coll} distribution. However, this method does not take into account any variation in the *dynamics* that may occur over the range of experimental collision energies that could result in different product angular distributions, product internal energy distributions, complex lifetimes and/or reactive cross sections depending on collision energy. Traditionally, these effects have been assumed to be small over the small range of collision energies in a typical crossed-beam experiment.

Instead of the *ad hoc* method of Gaussian convolution, in this study we explicitly test whether the effect of variation of the dynamics is really negligible. To this end we performed QS and QCT calculations in which the collision energies were dispersed (referred to as "dispersed" in the results below), as in the experiments, in addition to those done at fixed collision energies (which, combined with the traditional Gaussian convolution, will be referred to as "fixed" below). The calculations simulated the experimental collision energy distributions as follows: In the QS dispersed E_{coll} calculations, separate calculations were performed at various fixed E_{coll}. Product $P(\theta)$s and $P(E_t)$s were then calculated by a weighted average over the experimental distribution of collision energies. In the QCT dispersed E_{coll} calculations, trajectories were initiated with the experimental distribution of collision energies via Monte Carlo sampling. In these dispersed E_{coll} calculations, any differences in product $P(\theta)$s and $P(E_t)$s were included in the calculation, and $P(E_t)$s at different E_{coll} were obtained from product translational energies that were calculated directly for each trajectory from its specific E_{coll} and product rovibrational energy. In both the QS and QCT dispersed E_{coll} calculations, there was no need for the *ad hoc* Gaussian convolution employed in the fixed E_{coll} calculations since variation arising from a range of experimental collision energies was calculated explicitly.

In order to provide accurate experimental collision energy distributions for use in the dispersed E_{coll} QS and QCT calculations described above, the shape and width of the experimental collision energy distributions were calculated (using MATLAB®) from experimentally measured angular and velocity distributions of the beams as follows. Both initial reactant incident angles and one reactant initial velocity were selected via Monte-Carlo sampling of the two beam angular distributions (Gaussian) and one velocity distribution (speed ratio equation). Then, given the relative timing of the beams, the velocity of the second reactant

required for a collision to occur was calculated and the probability of the resulting collision energy was weighted by the probability of having a molecule with that velocity available (according to the experimental velocity distribution). These calculations produced experimental collision energy distributions with shapes that were indistinguishable from Gaussian distributions with $\sigma = 0.41$ for $E_{coll} = 7.3$ kcal/mol and $\sigma = 0.35$ for $E_{coll} = 5.7$ kcal/mol. These distributions were then used in the dispersed QS and QCT calculations with one modification: the calculations for 7.3 kcal/mol used a slightly larger σ (0.5 instead of 0.41). Since the widths themselves have some uncertainty, using $\sigma = 0.5$ produces a conservative upper limit for the magnitude of effects on the dynamics that arise from using our experimental distributions for E_{coll}.

III. RESULTS AND DISCUSSION

The background-corrected experimental TOF spectra for product $^{34}O_2$ from the $^{18}O + {}^{32}O_2$ isotope exchange reaction are shown as open circles in Figure 4 for $E_{coll} = 5.7$ kcal/mol and in Figure 5 for $E_{coll} = 7.3$ kcal/mol. A slower and a faster peak (or shoulder on the slower peak depending on laboratory angle) are evident at both collision energies, which we assign to the $^{18}O(^3P) + {}^{32}O_2(^3\Sigma_g^-) \rightarrow {}^{16}O(^3P) + {}^{34}O_2(^3\Sigma_g^-)$ reaction on the $O_3(X^1A')$ PES: the fast peak corresponds to $^{34}O_2$ produced in its ground vibrational state (v = 0) and the slower peak corresponds to the first vibrationally excited state (v = 1). Collisions of $O(^1D)$ with O_2 are not expected to contribute to the observed signal, based on the relevant energetics, geometries of the crossing between the relevant PESs, and comparisons with experiments using photolysis of ^{18}O-labeled SO_2, which produces only $O(^3P)$, as described in detail in Van Wyngarden *et al.*[15]

The lines in Figures 4 and 5 show the best-fit empirical simulations of the TOF spectra using the iterative forward convolution method described above: the heavy solid lines show the best fit for the total scattering, which is comprised of the v = 1 channel (light solid lines) and the

v = 0 channel (dashed lines). In these fits, the v = 1 channel accounts for 7.5% of the scattering for E_{coll} = 5.7 kcal/mol (Fig. 4) versus 8.3% for E_{coll} = 7.3 kcal/mol (Fig. 5). The underlying angular and translational energy distributions for these best fits to the TOF spectra are shown by the heavy solid lines in Figure 6 (for P(θ)) and Figure 7 (for $P(E_t)$). Finally, the convolution of the empirical P(θ)s and $P(E_t)$s for the v = 0 and v= 1 channels are shown as 3D product velocity flux diagrams in Figure 8 for E_{coll} = 5.7 kcal/mol and Figure 9 for E_{coll} = 7.3 kcal/mol.

The experimental product angular and translational energy distributions obtained from empirical fits to the $^{18}O + {}^{32}O_2$ isotope exchange TOF data at the two different collision energies are quite similar to each other and share the two main characteristics noted in Van Wyngarden *et al.*[15] for the 7.3 kcal/mol results: First, the best-fit total $P(E_t)$s at both collision energies (Figure 7A and D) peak near the collision energy limit, corresponding to low rovibrational excitation of the isotope exchange product $^{34}O_2$. Second, the best-fit P(θ)s have both forward and backward peaks but are biased toward the forward direction at both collision energies, as evident in Figures 6, 8, and 9. The forward bias indicates non-statistical behavior – in other words, indicating an O_3* complex that is short-lived with respect to its rotational period and, hence, that IVR is likely incomplete before dissociation occurs. The conservative uncertainty estimates for the empirical P(θ)s for E_{coll} = 7.3 kcal/mol given by the gray-shaded regions in Figure 6C and D show that this forward bias is quite robust for the v = 1 channel. In addition, although forward/backward symmetry is within the conservative estimate of the range of uncertainty for the empirical P(θ) for the v = 0 channel, we note that using a forward/backward symmetric P(θ) for this channel to simulate the TOF data requires that the P(θ) for the v = 1 channel have no backward peak whatsoever, which would indicate even more dramatic non-statistical behavior.

In addition to the similarities, there are also detectable differences between the experimental results for the two collision energies. For example, the forward bias in scattering for the v = 1 channel is less pronounced at 5.7 kcal/mol than at 7.3 kcal/mol, as is evident in Figure 10A, which shows the empirically-derived P(θ)s for the v = 1 channel at both collision energies on the same plot. The forward scattering between 0° and 35° in the empirical P(θ) for the 5.7 kcal/mol data lies largely below the conservative empirical fit range for 7.3 kcal/mol. This conclusion is expected to be robust since the uncertainty in P(θ) for v = 1 at E_{coll} = 5.7 kcal/mol should be substantially smaller than that at 7.3 kcal/mol because the v = 1 and v = 0 channels are better separated at the lower collision energy. This smaller bias towards forward scattering at a lower collision energy is consistent with a simple complex lifetime argument: Less energy is imparted to the collision complex at lower collision energies, allowing the collision complex to live longer, have more time to rotate, and consequently display a more symmetric angular distribution.

To gain more rigorous physical insight into any non-statistical effects in the O + O_2 isotope exchange reaction beyond these descriptive complex-lifetime arguments, the experimental results can be compared to the theoretical predictions of the QS and QCT models using both fixed E_{coll} and dispersed E_{coll}. The theoretical results are shown alongside the results derived from experiments in Figures 6 through 10, while comparisons of the experimental TOF spectra with the TOF spectra that have been simulated using the angular and translational energy distributions predicted by the QS and QCT methods are given in the supplemental material.[26]

Comparison of the experimental angular distributions with the QS and QCT results yields the following insights. As expected, the QS calculations cannot reproduce the experimental forward-scattering bias in the angular distributions (identical for fixed and dispersed E_{coll}) at

either collision energy (Figure 6, red lines) since they assume a long-lived complex and therefore necessarily result in scattering that is forward/backward symmetric. Unlike the QS model, the QCT method is, of course, able to take dynamics on the $O(^3P)+O_2$ PES into account and does not assume statistical behavior. The QCT calculations (fixed and dispersed E_{coll}) result in strong forward scattering biases for both v = 0 and v = 1 at both collision energies, with forward biases that are larger than those in the empirical P(θ)s at both collision energies (Fig. 6) and that are well outside the uncertainty range of the 7.3 kcal/mol empirical fit (Fig. 6C and D). Although there are some differences between the P(θ)s predicted by the fixed and dispersed E_{coll} calculations, especially for v = 1, their overall effects on the TOF simulations are small and do not substantially alter the discrepancies (nor consistencies) with experiment. The overprediction of the forward bias is also evident in the QCT simulations of the TOF data (see Figures S4 and S8 in the supplemental material[26]). For example, at 5.7 kcal/mol, the large QCT forward bias results in underprediction of the v = 1 TOF signal at angles that correspond to sideways and backward scattering regions (35°, 50° and 55°) and underprediction of the v = 0 channel in sideways scattering regions (50° and 55°). Furthermore, these large forward scattering biases predicted by the QCT method (fixed and dispersed) are larger at E_{coll} = 5.7 kcal/mol than at E_{coll} = 7.3 kcal/mol for both v = 0 and v = 1 (Fig. 10B and C), in contrast to the experimental trend (Fig. 10A). Although the small differences between the P(θ)s at 7.3 and 5.7 kcal/mol predicted by the QCT method may be within the statistical error of the calculations due to a limited number of trajectories, results of QCT calculations over a larger range of collision energies from 0.005 to 10 kcal/mol (Figure 11) indicate that the forward bias is near its maximum in the experimental collision energy range. Specifically, the forward bias is smaller both at very low E_{coll} (although it remains appreciable even at the lowest examined energy of 0.005 kcal/mol) and

at higher E_{coll} than those studied experimentally here (i.e., the QCT-calculated forward bias decreases simultaneously with the reduction in the reactive cross section at higher E_{coll}). These QCT results are intriguing since, given the simple argument presented earlier, lower collision energies are expected to result in longer-lived complexes which are more likely to rotate for more cycles and to display more statistical behavior – i.e., forward/backward symmetric peaking. While the fraction of complexes with lifetimes longer than 1 ps is indeed slightly larger in the QCT calculations for E_{coll} = 5.7 kcal/mol than for E_{coll} = 7.3 kcal/mol (28% and 25%, respectively), the calculated angular distributions are more forward-biased at 5.7 kcal/mol (Fig. 10B and C). Interestingly, the QCT calculations shown by Sun *et al.*[27] for the $^{16}O(^3P)$ + $^{32}O_2$ atom exchange reaction at the much lower collision energies of 0.7 and 1.2 kcal/mol also show a slight increase in forward bias at the lower of these two collision energies. In summary, although the QCT calculations correctly predict the occurrence of forward-scattering biases at collision energies of 5.7 and 7.3 kcal/mol, they overestimate the magnitudes of the forward bias as compared to our experimental data and do not predict the experimental trend of increasing forward bias with increasing collision energy. The specific reasons for these discrepancies are not yet clear, indicating the need for further improvements in the QCT calculations and/or the PES.

In addition to comparing angular distributions, comparison of experimental product translational energy distributions, $P(E_t)$s, with the QS and QCT fixed E_{coll} calculations yields the following insights. First we note that the QS and QCT calculations predict very similar $P(E_t)$s that capture the main features of the experimental $P(E_t)$s, which peak near the collision energy limits, as demonstrated by the correct prediction of the timing of the peaks in the TOF spectra (see Figures S1, S3, S5 and S7 in the supplemental material[26]) and the similarity of the calculated

$P(E_t)$s to those derived empirically from the measurements (Figure 7). Despite these general similarities, however, there are significant differences between the experimental results and the QS and QCT fixed E_{coll} predictions for the TOF spectra, the total $P(E_t)$s, and the $P(E_t)$s for the v = 0 and v = 1 channels. Specifically, the QS and QCT calculations underestimate scattering at long TOFs for both collision energies (>200 μs for 5.7 kcal/mol and >170 μs for 7.3 kcal/mol; see Figs. S1 and S5 in the supplemental material[26]) implying underestimation of the amount of product $^{34}O_2$ with high rovibrational excitation. Indeed, Figure 7D shows that the QS and QCT fixed E_{coll} predictions for the total $P(E_t)$ for E_{coll} = 7.3 kcal/mol are well below the range of uncertainty for the empirical fit for most of the range of E_t below 6 kcal/mol and well above the empirical range for E_t above 6 kcal/mol; Figure 7A shows that the discrepancy is even larger for E_{coll} = 5.7 kcal/mol (for which the uncertainty in the empirical fit is expected to be smaller than that for E_{coll} = 7.3 kcal/mol, as noted earlier).

Although this underestimation of products with low E_t by the QS model could be attributed to non-statistical rovibrational energy distributions in the experiment, as previously suggested for the 7.3 kcal/mol experimental results,[15] our new dispersed E_{coll} calculations demonstrate that most of the discrepancy can be accounted for by performing calculations with the experimental collision energy distributions instead of with fixed collision energies at the average experimental collision energy. In fact, overall the dispersed E_{coll} results from both QS and QCT match experiment much better than the fixed E_{coll} results since they predict less strongly peaked (wider) total $P(E_t)$s shifted toward slower (lower E_t) products (Figures 7A and D, dotted lines). Middle-range translational energy products (that were underpredicted by fixed E_{coll} calculations) are increased by more slow v = 0 products (Figures 7B and E) and, for QCT, also by more fast v = 1 products (Figures 7C & F). This improvement is most easily seen in

Figures 7A and D (5.7 and 7.3kcal/mol, respectively), where the less sharply peaked dispersed E_{coll} total $P(E_t)$'s are overall closer to the empirical fit range, with the notable exception of the very highest translational energies for the QCT results. The improvement can also be seen in simulated TOF peaks (especially v = 0) that are wider on the slow side and consequently do not underpredict slow products as much as the fixed E_{coll} simulations did (comparing Figures S1 vs. S2 and S3 vs. S4 in the supplemental material[26] for QS and QCT respectively for 5.7 kcal/mol and, similarly, S5 vs. S6 and S7 vs. S8 for 7.3 kcal/mol). Widening the v = 0 peaks on the slow side consequently lowers them and shifts them to longer TOF, which also improves angles of 10°, 15°, 20° for 7.3 kcal/mol and 20°, 25° and 35° for 5.7 kcal/mol where the v = 0 peak had been overpredicted and/or too fast. Interestingly, the v = 1 / v = 0 branching ratios remain essentially the same for the dispersed versus fixed E_{coll} calculations (see Figures 8 and 9), so changes in the TOF peaks and the total $P(E_t)$s are due to changes in the shapes for the v = 0 and v = 1 P(E)s and not their relative contributions.

Although the QS and QCT dispersed E_{coll} results for the $P(E_t)$s are not in complete agreement with the empirical $P(E_t)$s, overall the dispersed E_{coll} calculations provide substantial improvements in agreement with experiment over those with fixed E_{coll} since the dispersed E_{coll} calculations produce wider $P(E_t)$s shifted toward lower translational energies. In fact, the agreement between theoretical and experimental $P(E_t)$s is close enough that further improvements in the theoretical $P(E_t)$s would not result in significant improvement in TOF simulations of the data without first improving theoretical $P(\theta)$s. Therefore, the major remaining discrepancies between the empirical and theoretical TOF simulations are due to differences in the angular distributions – specifically, QS angular distributions that lack a forward bias or QCT angular distributions that are too strongly forward biased – so efforts to further improve

theoretical calculations should focus on improving P(θ)s. The origin of the improvements in agreement between the experimental and theoretical $P(E_t)$s by using the dispersed E_{coll} distributions in the QS and QCT calculations is likely due to the fact that the dispersed E_{coll} distributions can account for (a) larger reactive cross sections for collisions with lower E_{coll} resulting in lower product translational energies, (b) possible variation in final rovibrational distribution as a function of E_{coll}, and (c) variation in the amount of reactant translational energy available for distribution into product translational energy. In contrast, the Gaussian convolution method for fixed E_{coll} can only account for (c). Importantly, the substantial improvements in agreement between theoretical and empirical $P(E_t)$s when using dispersed E_{coll} calculations to take all three of these effects into account suggest that theoretical calculations for other experimental systems may result in similar improvements if the experimental collision energy distributions are simulated directly.

Although using dispersed E_{coll} distributions in the QS and QCT calculations result in improved $P(E_t)$s, some insights can still be obtained from a detailed examination of the remaining differences between theoretical and empirical $P(E_t)$s. Although the $P(E_t)$s for $v = 0$ from the QS dispersed E_{coll} calculations are in good agreement with experiment (Figure 7B and E), the calculated total $P(E_t)$s show that the slowest products (< 2.5 kcal/mol and < 3 kcal/mol in Figures 7A and D, respectively) corresponding to the highest rovibrational excitation are still underpredicted. Importantly, the new 5.7 kcal/mol data can be used to determine whether this underestimation of rovibrationally excited products is due to underestimation of rotational excitation, vibrational excitation, or both since the $v = 0$ and $v = 1$ channels are better separated in the TOF spectra than at 7.3 kcal/mol, thus providing a tighter lower bound on the $v = 1$ branching ratio. The branching ratio at 5.7 kcal/mol for the $v = 1$ channel from the QS model is

3.3%, which is quite low compared to the empirical value of 7.5%. Indeed, although the data can be fit with a range of empirical v = 1 branching ratios, it is impossible to simulate the experimental data using a v = 1 branching ratio of 3.3%. We therefore conclude that the underestimation of product $^{34}O_2$ with high rovibrational excitation by the QS method is at least partially due to underestimation of high (v = 1) *vibrational* excitation, which may indicate that the vibrational distributions in the experiments are non-statistical.

Interestingly, these differences in rovibrational excitation between the experimental results and the QS (dispersed E_{coll}) predictions are larger at E_{coll} = 5.7 kcal/mol than at E_{coll} = 7.3 kcal/mol, with the QS calculation only accounting for approximately one third of the 5.7 kcal/mol TOF signal for times >200 μs at 20-35° (Fig. S6 in the supplemental material[26]; see also Fig. 7A) while accounting for at least two thirds of the 7.3 kcal/mol signal for times >170 μs at 20-35° (Fig. S2; see also Fig. 7D). Thus, the experimental product internal energy distribution appears to be less statistical at the lower collision energy, an intriguing trend, if real, particularly since the experimental angular distributions were already shown above to exhibit the opposite trend – that is, becoming more statistical (less forward-biased) with lower collision energy (e.g., Figure 10A). In contrast, it is worth mentioning that the QCT calculations for the vibrational energy distribution (discussed below) and the forward bias show the same trend: less statistical behavior at the lower collision energy for both (even though the differences may be within the statistical error bars).

Although the $P(E_t)$s predicted by the dispersed E_{coll} QCT calculations are overall very similar to the dispersed E_{coll} QS calculations, the QCT method results in more $^{34}O_2$ in the v = 1 state than the QS model at both collision energies (5.4% vs. 3.3%, respectively, for 5.7 kcal/mol and 10.1% vs. 8.2% for 7.3 kcal/mol). Therefore it better reproduces the experimental vibrational

distributions – specifically, more scattering at TOFs > 200 μs and better agreement (i.e., within the uncertainty range for the 7.3 kcal/mol empirical fit) with the empirical fits for the v = 1 peaks of the total $P(E_t)$s (Figures 7A and D). However, the QCT method still underpredicts scattering at medium and low translational energy (e.g. < 5.5 kcal/mol for E_{coll} = 5.7 kcal/mol), indicating that, although it correctly predicts high vibrational excitation, it underestimates highly rotationally-excited $^{34}O_2$ in the v = 0 state. In summary, while the QS method underestimates high vibrational excitation, the QCT method can reproduce the experimental vibrational state distributions but not the experimental rotational state distributions. The differences in vibrational excitation between the experimental results and the QS predictions could be interpreted as deviations from statistical behavior or they could result from errors in the ground state PES used in the QS method and/or from contributions from excited-state PESs that are neglected in the QS calculations. However, since both the QS and QCT methods used the same PES and assume no non-adiabatic effects, the ability of the dynamic QCT method to correctly predict high vibrational excitation suggests that the QS model underprediction of v = 1 indeed indicates that the experimental vibrational distribution is non-statistical.

In summary, although the QCT method correctly predicts the occurrence of non-statistical effects (i.e., bias toward forward scattering and higher vibrational excitation than the statistical prediction), the non-statistical forward bias is overestimated while the product rotational excitation is underestimated as compared with the experiments. Furthermore, in both cases the differences between the $P(\theta)$s and $P(E_t)$s from the QCT predictions and the experimental results are larger at E_{coll} = 5.7 kcal/mol than at E_{coll} = 7.3 kcal/mol. Compare, for example, $P(\theta)$s for the v = 1 channel in Figure 6B and D and the total $P(E_t)$s in Figure 7A and D at both collision energies, noting that uncertainties in the empirical fits for the 5.7 kcal/mol data

are smaller than those for the 7.3 kcal/mol data for all but the P(θ) fit for the v = 0 channel. This inability of the QCT method to predict the experimental trends with E_{coll} in both the non-statistical forward bias and the high rotational excitation of the product scattering in the $^{18}O + {}^{32}O_2$ isotope exchange reaction shows that the QCT method using the Babikov *et al.*[17] PES does not completely capture the dynamic behavior of $^{18}O + {}^{32}O_2$ isotope exchange and that further improvements in theoretical treatments and/or electronic structure are required to explain the measurements of non-statistical behavior in the $O + O_2$ scattering experiments. Indeed, several newer ozone PESs have been proposed recently.[28,29,30] In particular, Dawes *et al.*[31] have demonstrated that the submerged reef structure in the entrance and exit channels of the O_3 PES is due to artifacts of the electronic structure methods used to compute the PES. The new PES of Dawes *et al.* yielded a much better agreement with the measured rate constants and, perhaps more importantly, correctly predicted the negative temperature dependence of the exchange rate constants.[30] The absence of the submerged reef structure in the latest PES could conceivably change the lifetime of the O_3^* intermediate complex. However, we chose to use the old PES of Babikov *et al.* so that we can compare with our earlier results. Future quantum dynamical calculations on the new PES should provide much needed information concerning the lifetime and state-to-state reaction dynamics of this important reaction and perhaps answer some of the questions raised by the current study, as well as remaining questions surrounding the unusual isotopic composition of ozone,[32] which is highly enriched in both ^{17}O and ^{18}O.

The non-statistical effects in the $O(^3P)+O_2$ isotope exchange reaction – the forward-scattering bias and the possibility of non-statistical product vibrational distributions – also have implications for quantum statistical theories in general, which have recently been applied successfully to many similar barrierless reactions with deep wells.[20,21,25,33,34,35,36,37] Although one

of these quantum statistical models was successfully used to simulate TOF spectra from two other deep-well reactions (i.e., those for $N(^1D) + H_2 \rightarrow NH + H$ [25] and for $C(^1D) + H_2 \rightarrow CH + H$ [33]), the observation of non-statistical forward-scattering bias in the $^{18}O + {}^{32}O_2$ experimental TOF spectra presented here clearly indicates that the statistical assumption of the quantum statistical technique may not be valid for all deep-well reactions. The reason for the failure of the statistical assumption for the $^{18}O + {}^{32}O_2$ isotope exchange reaction may be that the well-depth is only 26 kcal/mol compared to 126 and 99 kcal/mol with respect to reactants for $N(^1D) + H_2$ and $C(^1D) + H_2$, respectively. This smaller well-depth may result in a shorter-lived collision complex for which the statistical assumption of complete IVR is not valid, at least at the collision energies probed here. Indeed, recent dynamically exact quantum mechanical calculations of reactive scattering for the $O + O_2 \rightarrow O_2 + O$ reaction at collision energies of 0 to 2 kcal/mol[27] and for the $H + O_2 \rightarrow HO + O$ reaction[38] show that neither reaction is statistical despite their complex-forming reaction mechanism, even at these much lower collision energies, but that $H + O_2$ behaves more statistically than $O + O_2$, most likely due to its deeper potential well (55 kcal/mol vs 26 kcal/mol) and the weak vibrational anharmonicity of O_3. For $O + O_2$, Sun *et al.*[27] interpreted the combination of their quantum dynamics and QCT calculations to indicate that the non-statistical character in both the forward scattering bias and the energy redistribution can be traced to a large fraction of short-lived "osculating" complexes which live for at least 4 vibrational periods, as well as some complexes which are long-lived and behave statistically – an interpretation that is consistent both with the experimental results shown here at much higher collision energies and with the discrepancies between the experimental results and the QS calculations presented here.

V. CONCLUSIONS

Reactive scattering experiments were performed for the $^{18}O + {}^{32}O_2$ isotope exchange reaction at two collision energies (5.7 and 7.3 kcal/mol) in order to examine the collision energy dependence of the non-statistical effects revealed in the 7.3 kcal/mol experiments presented in Van Wyngarden *et al.*[15] and to test their robustness given uncertainties due to the width of the experimental collision energy distribution. The experimental results were also compared to predictions from quantum statistical and quasi-classical trajectory calculations with both fixed and dispersed collision energies, both at E_{coll} = 5.7 and 7.3 kcal/mol. The comparison to QS predictions allowed the identification of possible non-statistical effects while the comparison to the QCT predictions allowed evaluation of the ability of the QCT technique using the Babikov *et al.*[17] PES to predict the dynamic behavior of $O + O_2$ isotope exchange. Employing the experimental collision energy distribution instead of a fixed collision energy in both QS and QCT calculations resulted in marked improvement in the agreement in results between both theoretical treatments and experiment and, therefore, may be expected to improve theoretical predictions of crossed-beam data for other systems.

The TOF data at the two collision energies were very similar to each other and showed that the two non-statistical effects measured in the 7.3 kcal/mol experiments persisted at the lower collision energy of 5.7 kcal/mol. First, at both collision energies, the scattering displayed a forward bias that could not be reproduced in the QS model since the statistical assumption necessarily yields forward/backward symmetric scattering. This inability of the QS method to describe reactive scattering in the $O + O_2$ isotope exchange reaction demonstrates a limit to the applicability of quantum statistical models to deep-well reactions. Second, although the new QS dispersed E_{coll} rotational distributions agree with experiment, the experimental vibrational

distributions of the O_2 products are probably non-statistical since they have higher v = 1 / v = 0 ratios than that predicted by the quantum statistical (QS) calculation. Intriguingly, the energy dependence of these two non-statistical effects observed in the experiments were opposite: the bias toward forward scattering was less pronounced at 5.7 kcal/mol than at 7.3 kcal/mol, while the non-statistical vibrational distribution was more pronounced at 5.7 kcal/mol.

These non-statistical effects were further examined by comparing the scattering data to QCT predictions. Although the QCT calculations correctly predicted forward-biased scattering and captured the experimental product vibrational energy distribution better than the QS method, QCT results were inconsistent with experiments in the following ways: Most importantly, QCT overpredicted the forward scattering bias; additionally, it underpredicted rotationally-excited products and produced larger non-statistical effects at the lower of the two collision energies both in product angular and vibrational energy distributions in contrast to the experiment, which showed the same vibrational energy trend, but the opposite angular distribution trend. These discrepancies all indicate that the dynamics calculations do not completely capture the dynamic behavior observed in the experiment. The energy-dependent $^{18}O + {}^{32}O_2$ scattering results therefore clearly showed that (1) the basic "statistical" assumption of the QS method is not fulfilled and (2) the QCT method using the Babikov *et al.*[17] $O_3(X^1A')$ PES also does not reproduce the measured $O + O_2$ scattering data (especially angular distributions). These observations further underscore the need, noted previously in Van Wyngarden *et al.*,[15] for improvement in the quality of the $O_3(X^1A')$ PES used and/or in the theoretical treatment of dynamics. The set of experimental scattering data at two different collision energies presented here, in combination with experimental collision energy distributions (based on Monte Carlo

calculations) shown to improve theoretical calculations, provide important benchmarks to guide these improvements.

ACKNOWLEDGMENTS

We gratefully acknowledge support from the US National Science Foundation (CHE - 0809973 to KB), the US Department of Energy (DE-FG02-05ER15694 to HG), the National Natural Science Foundation of China (Grant No. 11274202 to SYL), the Hungarian Scientific Research Fund (OTKA K108966, to GL), the Hungarian National Development Agency (Grant No. KTIA_AIK_12-1-2012-0014, to GL), San José State University, San Jose, CA (start-up support for AV) and Academia Sinica, Taiwan.

REFERENCES

[1] S. M. Anderson, A. D. Hulsebusch, and K. Mauersberger, J. Chem. Phys. **107**, 5385 (1997).

[2] K. Mauersberger, B. Erbacher, D. Krankowsky, J. Gunther, and R. Nickel, Science **283**, 370 (1999).

[3] C. Janssen, J. Guenther, D. Krankowsky, and K. Mauersberger, J. Chem. Phys. **112**, 11109 (2000).

[4] C. Janssen, J. Guenther, K. Mauersberger, and D. Krankowsky, Phys. Chem. Chem. Phys. **3**, 4718 (2001).

[5] P. Fleurat-Lessard, S. Y. Grebenshchikov, R. Schinke, C. Janssen, and D. Krankowsky, J. Chem. Phys. **119**, 4700 (2003).

[6] J. A. Kaye and D. F. Strobel, J. Geophys. Res. **88**, 8447 (1983); J. A. Kaye, J. Geophys. Res. **91**, 7865 (1986).

[7] Y. Q. Gao and R. A. Marcus, Science **293**, 259 (2001).

[8] Y. Q. Gao and R. A. Marcus, J. Chem. Phys. **127**, 244316 (2007).

[9] M. Kryvohuz and R. A. Marcus, J. Chem. Phys. **132**, 224305 (2010).

[10] N. Ghaderi and R. A. Marcus, J. Phys. Chem. B **115**, 5625 (2011).

[11] R. Schinke and P. Fleurat-Lessard, J. Chem. Phys. **122**, 094317 (2005).

[12] R. Schinke, P. Fleurat-Lessard, and S. Y. Grebenshchikov, Phys. Chem. Chem. Phys. **5**, 1966 (2003).

[13] M. V. Ivanov and D. Babikov, Proc. Natl. Acad. Sci. USA. **110**, 17708 (2013).

[14] H. Guo, Int. Rev. Phys. Chem. **31**, 1 (2012).

[15] A. L. Van Wyngarden, K. A. Mar, K. A. Boering, J. J. Lin, Y. T. Lee, S. Y. Lin, H. Guo, and G. Lendvay, J. Am. Chem. Soc. **129**, 2866 (2007).

[16] S. Y. Lin and H. Guo, J. Phys. Chem. A **110**, 5305 (2006).

[17] D. Babikov, B. K. Kendrick, R. B. Walker, R. T. Pack, P. Fleurat-Lesard, and R. Schinke, J. Chem. Phys. **118**, 6298 (2003).

[18] J. J. Lin, D. W. Hwang, S. Harich, Y. T. Lee, and X. M. Yang, Rev. Sci. Instrum. **69**, 1642 (1998).

[19] J. J. Lin, S. Harich, Y. T. Lee, and X. Yang, J. Chem. Phys. **110**, 10821 (1999).

[20] E. J. Rackham, T. Gonzalez-Lezana, and D. E. Manolopoulos, J. Chem. Phys. **119**, 12895 (2003).

[21] E. J. Rackham, F. Huarte-Larranaga, and D. E. Manolopoulos, Chem. Phys. Lett. **343**, 356 (2001).

[22] S. Y. Lin and H. Guo, J. Chem. Phys. **120**, 9907 (2004).

[23] L. Bonnet, Int. Rev. Phys. Chem. **32**, 171 (2013).

[24] Á. Bencsura, G. Lendvay, J. Phys. Chem. A **116**, 4445 (2012).

[25] N. Balucani, P. Casavecchia, L. Banares, F. J. Aoiz, T. Gonzalez-Lezana, P. Honvault, and J. M. Launay, J. Phys. Chem. A **110**, 817 (2006).

[26] See supplemental material at [URL will be inserted by AIP] for figures comparing the experimental TOF spectra with TOF spectra simulated by the QS and QCT methods."

[27] Z. G. Sun, L. Liu, S. Y. Lin, R. Schinke, H. Guo, and D. H. Zhang, Proc. Natl. Acad. Sci. USA **107**, 555 (2010).

[28] M. Ayouz and D. Babikov, J. Chem. Phys. **138**, 164311 (2013).

[29] V. G. Tyuterev, R. V. Kochanov, S. A. Tashkun, F. Holka, and P. G. Szalay, J. Chem. Phys. **139**, 134307 (2013).

[30] R. Dawes, P. Lolur, A. Li, B. Jiang, and H. Guo, J. Chem. Phys. **139**, 201103 (2013).

[31] R. Dawes, P. Lolur, J. Ma, and H. Guo, J. Chem. Phys. **135**, 081102 (2011).

[32] K. L. Feilberg, A. A. Wiegel, K. A. Boering, Chem. Phys. Lett. **556**, 1 (2013).

[33] N. Balucani, G. Capozza, E. Segoloni, A. Russo, R. Bobbenkamp, P. Casavecchia, T. Gonzalez-Lezana, E. J. Rackham, L. Banares, and F. J. Aoiz, J. Chem. Phys. **122**, 234309 (2005).

[34] M. H. Alexander, E. J. Rackham, and D. E. Manolopoulos, J. Chem. Phys. **121**, 5221 (2004).

[35] S. Y. Lin and H. Guo, J. Phys. Chem. A **108**, 2141 (2004).

[36] S. Y. Lin and H. Guo, J. Chem. Phys. **122**, 074304 (2005).

[37] S. Y. Lin, E. J. Rackham, and H. Guo, J. Phys. Chem. A **110**, 1534 (2006).

[38] Z. Sun, D. H. Zhang, C. Xu, S. Zhou, D. Xie, G. Lendvay, S.-Y. Lee, S. Y. Lin, and H. Guo, J. Am. Chem. Soc. **130**, 14962 (2008).

FIGURES

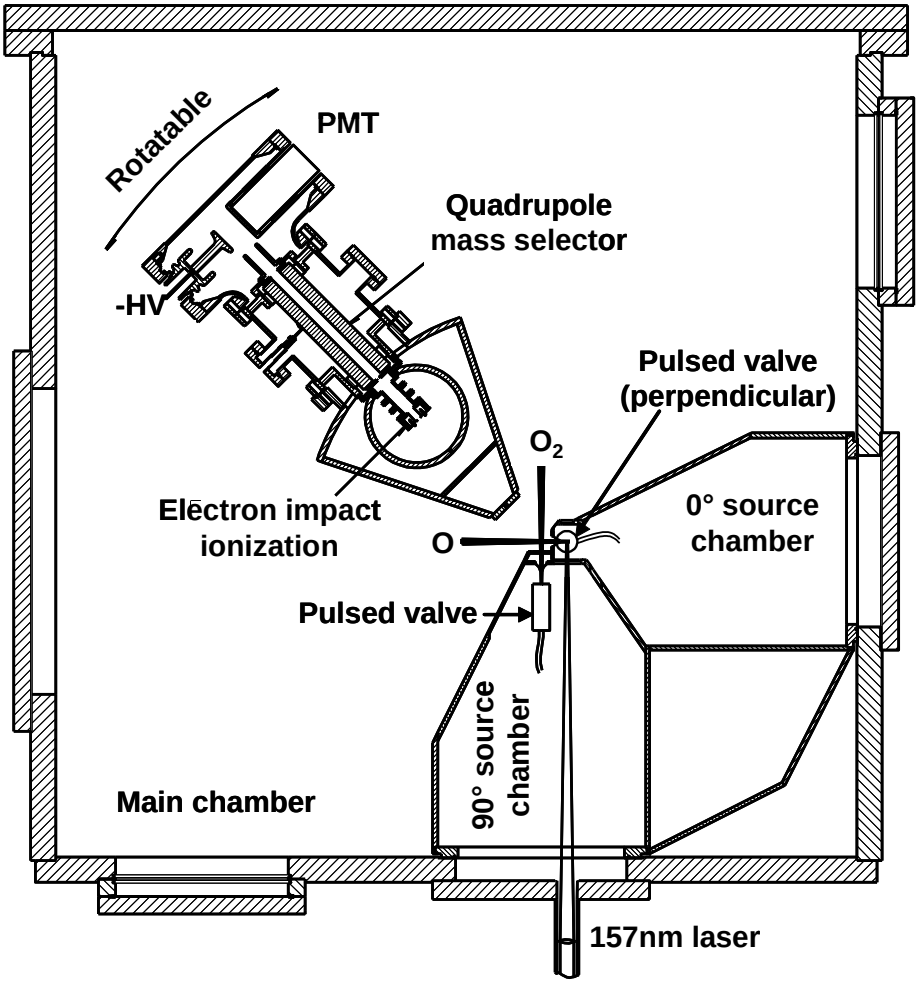

FIG. 1. Schematic of the crossed-beam apparatus viewed from above. For the 5.7 kcal/mol collision energy experiments, the orientation of the pulsed valve for the photolytic precursor $^{18}O^{18}O$ was perpendicular to the plane of reaction, as shown. For the 7.3 kcal/mol collision energy experiments, the orientation of the pulsed valve for the precursor $^{18}O^{18}O$ was tilted toward the interaction region (see text).

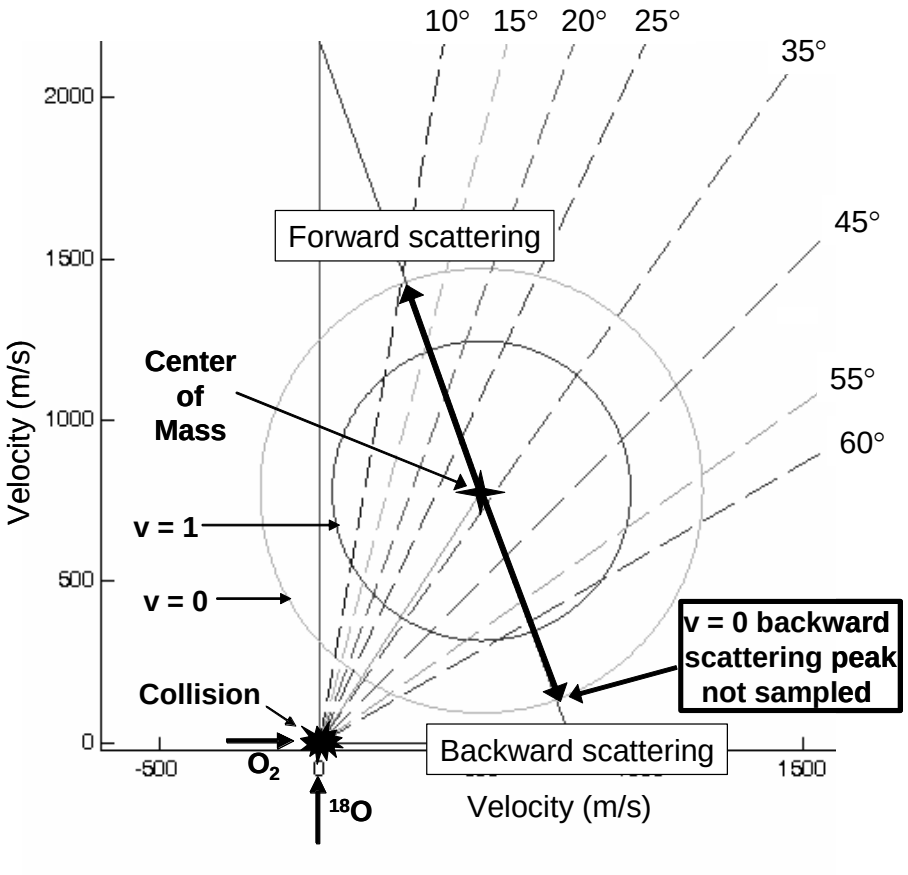

FIG. 2. Newton diagram for E_{coll} = 7.3 kcal/mol. The laboratory frame velocities that correspond to the centers of the $^{34}O_2$ v = 0 and v = 1 TOF peaks are represented by the two rings around the center-of-mass frame collision. The thick arrows denote the direction of forward and backward scattering. The detector is rotated around the lab-frame collision, so the dotted lines show which regions of the scattering were sampled by the detector at the angles where spectra were collected.

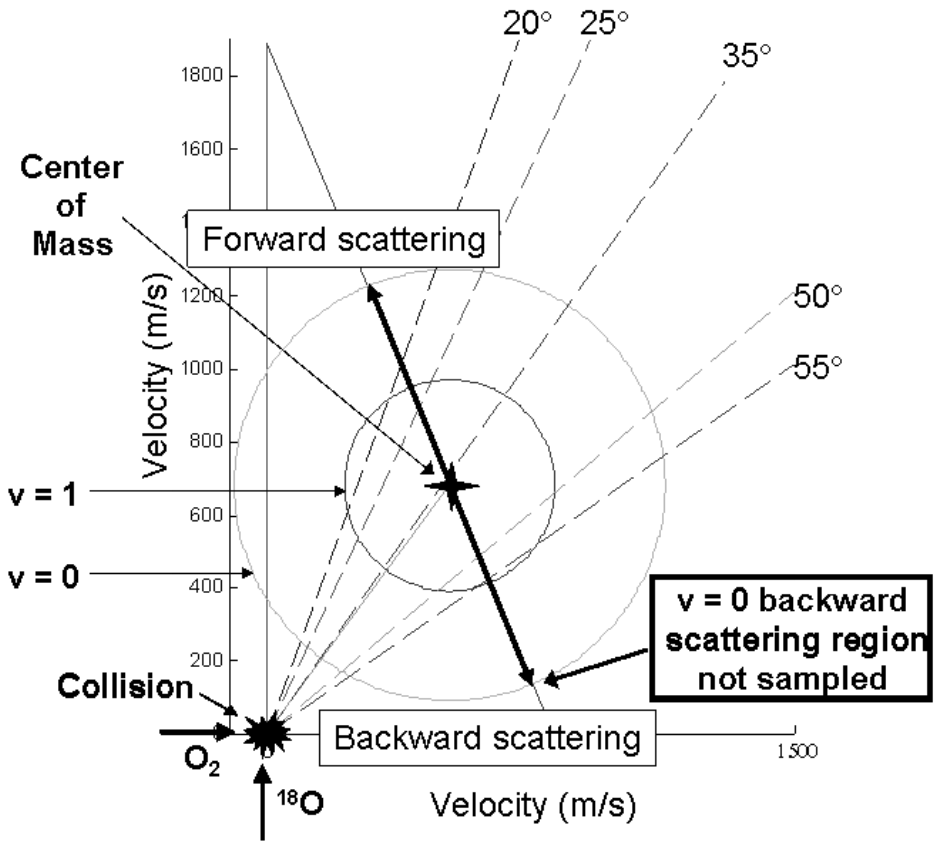

FIG. 3. Newton diagram for E_{coll} = 5.7 kcal/mol. See caption to Figure 2. Here spectra were collected at angles chosen to cover the angular distribution of the v = 1 channel only.

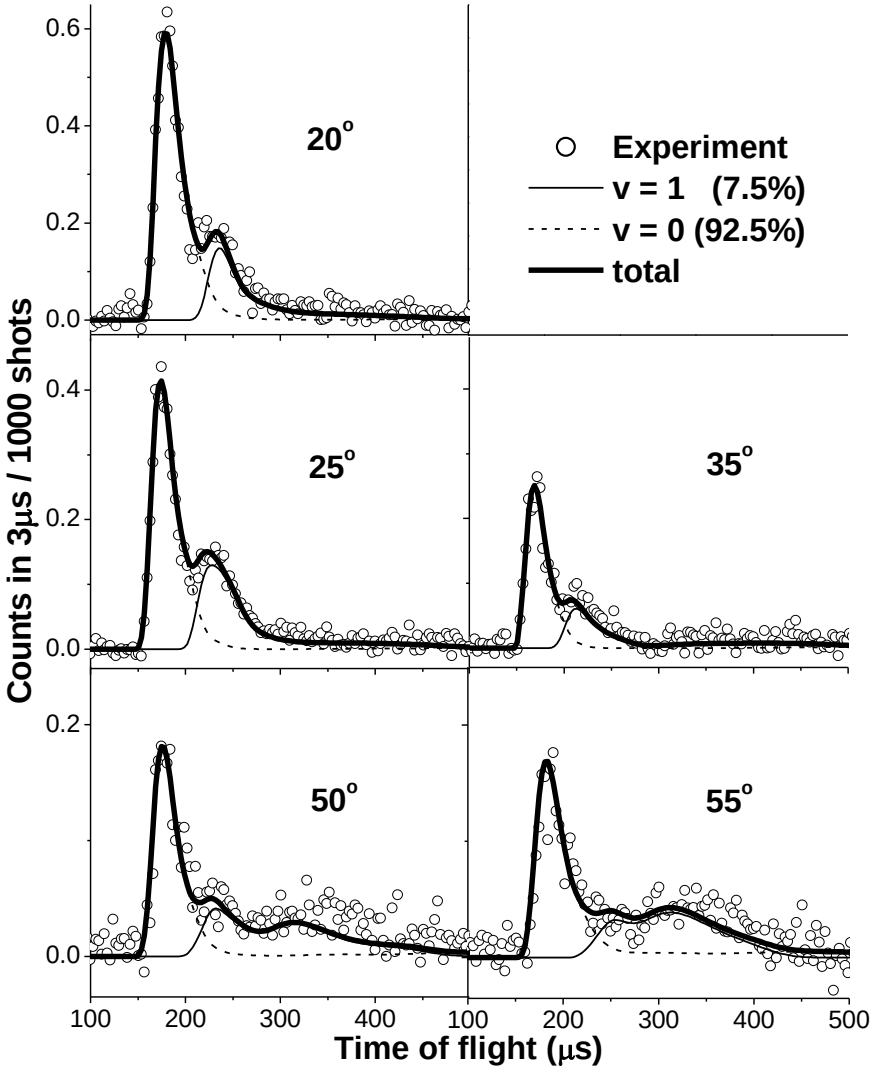

FIG. 4. Background-corrected time-of-flight spectra for m/z = 34 ($^{18}O^{16}O$) at 5 different laboratory angles for E_{coll} = 5.7 kcal/mol. Note different y-axis scales. Open circles are the experimental data; dashed and solid lines are the best-fit empirical simulation using the P(θ)s and P(E_t)s given by the black lines in Figures 6 and 7.

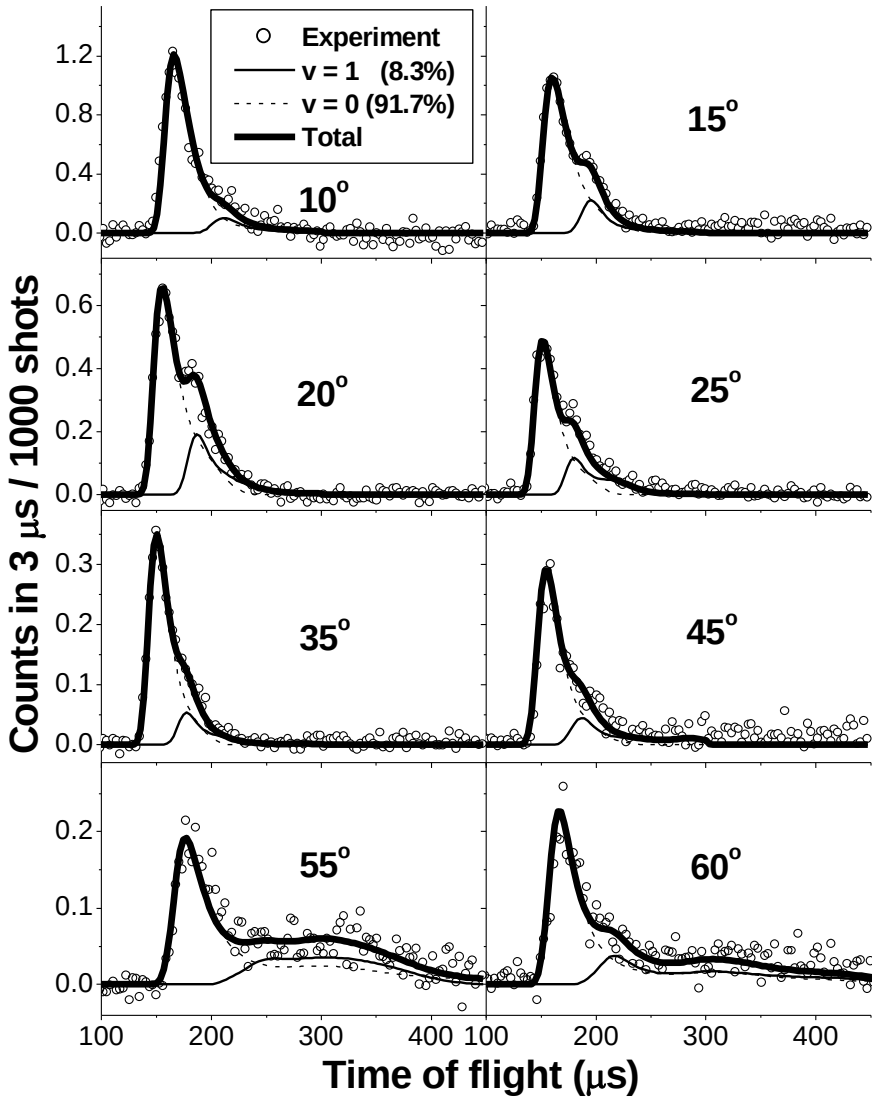

FIG. 5. Background-corrected time-of-flight spectra for m/z = 34 ($^{18}O^{16}O$) at 8 different laboratory angles for E_{coll} = 7.3 kcal/mol. Note different y-axis scales. Open circles are the experimental data; dashed and solid lines are the best-fit empirical simulation using the P(θ)s and P(E_t)s given by the black lines in Figures 6 and 7. [Reprinted with permission from A. L. Van Wyngarden, K. A. Mar, K. A. Boering, J. J. Lin, Y. T. Lee, S. Y. Lin, H. Guo, and G. Lendvay, J. Am. Chem. Soc. **129**, 2866 (2007). Copyright 2007 American Chemical Society.]

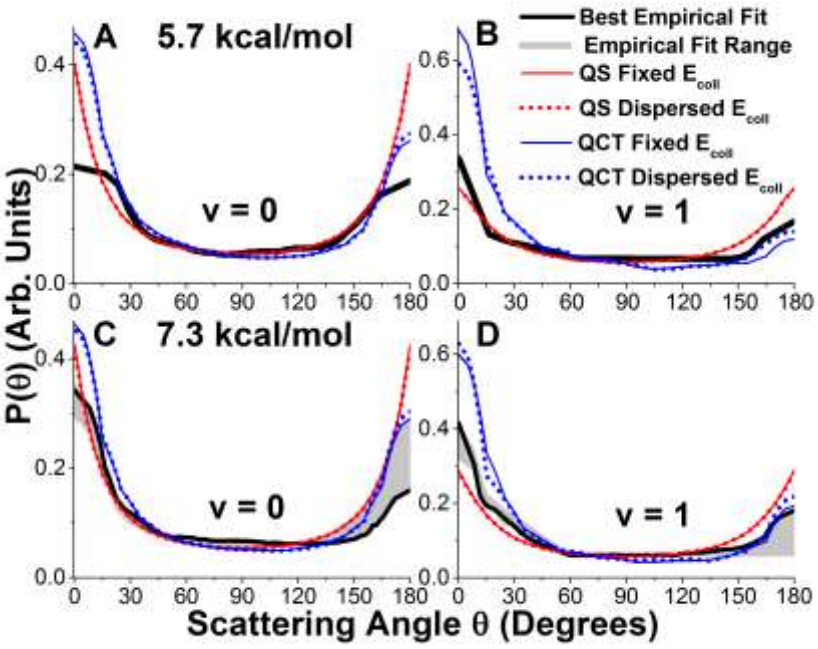

FIG. 6. Product angular distributions: The black lines are the P(θ)s used in the best-fit empirical simulations of the TOF spectra for (A) v=0 for 5.7 kcal/mol, (B) v=1 for 5.7 kcal/mol, (C) v = 0 for 7.3 kcal/mol, and (D) v=1 for 7.3 kcal/mol. The gray shaded regions are conservative estimates of the uncertainty corresponding to the ranges of adequate fits to the TOF spectra (see Methods section). The red and blue lines correspond to the QS and QCT predictions, respectively, while solid and dotted lines indicate fixed and dispersed E_{coll}, respectively. (Note different y-axes scales). [7.3 kcal/mol empirical and QS fixed E_{coll} results reprinted (adapted) with permission from A. L. Van Wyngarden, K. A. Mar, K. A. Boering, J. J. Lin, Y. T. Lee, S. Y. Lin, H. Guo, and G. Lendvay, J. Am. Chem. Soc. **129**, 2866 (2007). Copyright 2007 American Chemical Society.]

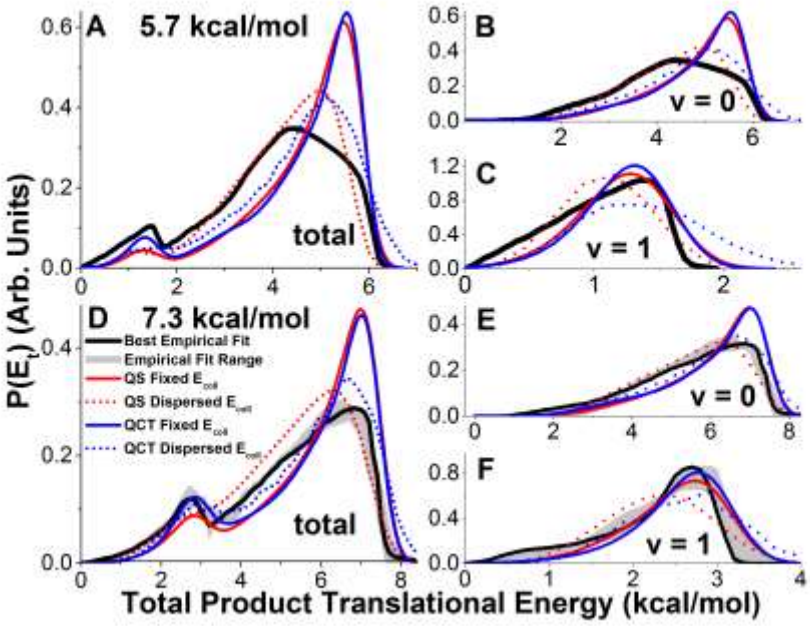

FIG. 7. Product translational energy distributions: The black lines are the $P(E_t)$s used in the best-fit empirical simulations of the TOF spectra for the 5.7 kcal/mol experiments (A, B, and C) and the 7.3 kcal/mol experiments (D, E, F). (A) and (D) show the total $P(E_t)$, (B) and (E) show $P(E_t)$ for v=0, and (C) and (F) show $P(E_t)$ for v=1. Areas under the separate v = 0 and v = 1 $P(E_t)$s were normalized to 1 so that rotational distributions for each vibrational state can be compared, while the relative contributions of the v = 0 and v = 1 channels are evident in the total $P(E_t)$s in (A) and (D). The gray shaded regions are conservative estimates of the uncertainty corresponding to the ranges of adequate fits to the TOF spectra (see Methods section). The red and blue lines correspond to the QS and QCT predictions, respectively, while solid and dotted lines indicate fixed and dispersed E_{coll}, respectively. (Note different x and y-axes scales). [7.3 kcal/mol empirical and QS fixed E_{coll} results reprinted (adapted) with permission from A. L. Van Wyngarden, K. A. Mar, K. A. Boering, J. J. Lin, Y. T. Lee, S. Y. Lin, H. Guo, and G. Lendvay, J. Am. Chem. Soc. **129**, 2866 (2007). Copyright 2007 American Chemical Society.]

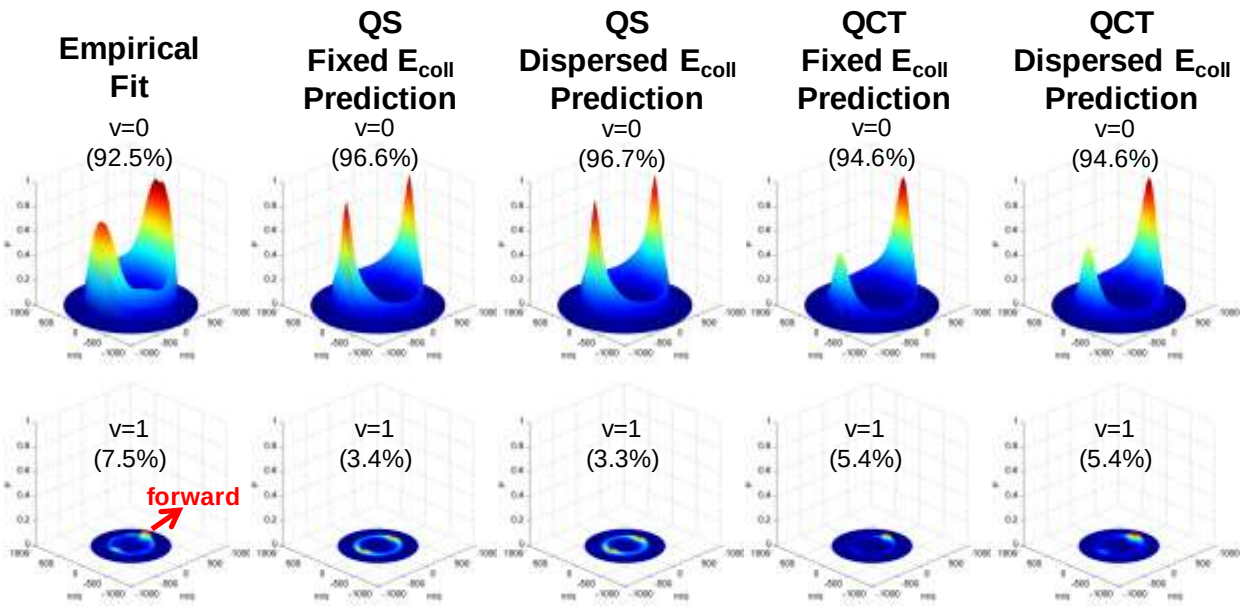

FIG. 8. Center of mass 3-D product velocity flux diagrams for E_{coll}=5.7 kcal/mol showing the convolution of the $P(E_t)$s and $P(\theta)$s used in the empirical, QS, and QCT simulations of the TOF data. QS and QCT results are shown using both fixed and dispersed E_{coll}. The probabilities have been normalized by the branching ratios shown for the v = 0 and v = 1 channels.

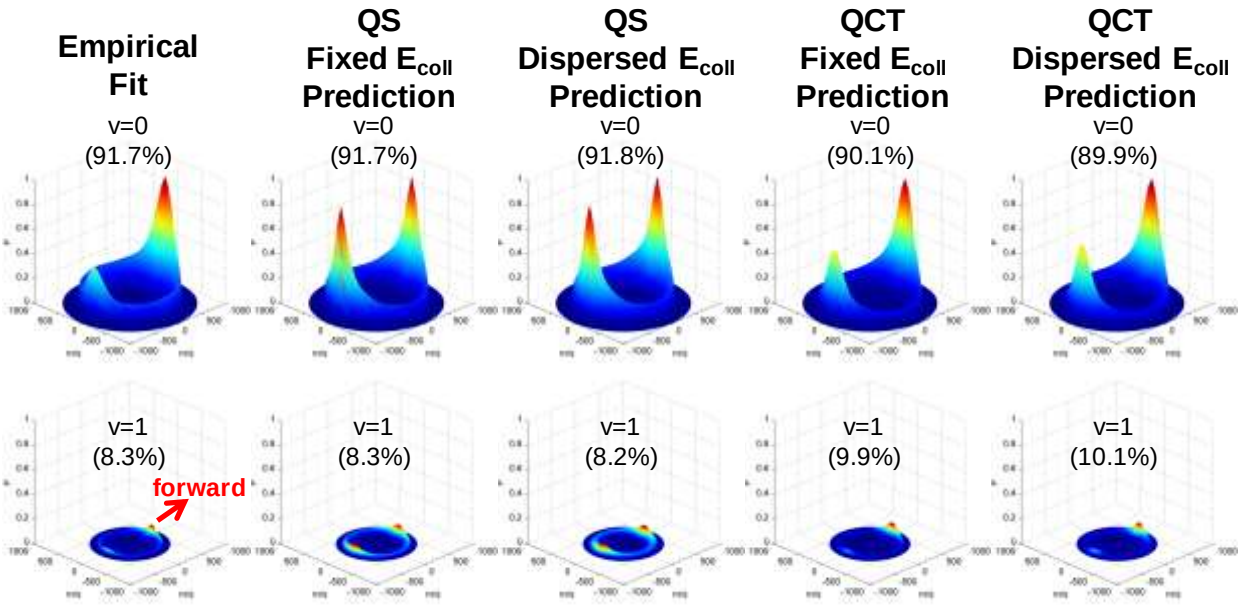

FIG. 9. Center of mass 3-D product velocity flux diagrams for E_{coll}=7.3 kcal/mol showing the convolution of the P(E_t)s and P(θ)s used in the empirical, QS, and QCT simulations of the TOF data. QS and QCT results are shown using both fixed and dispersed E_{coll}. The probabilities have been normalized by the branching ratios shown for the v = 0 and v = 1 channels.

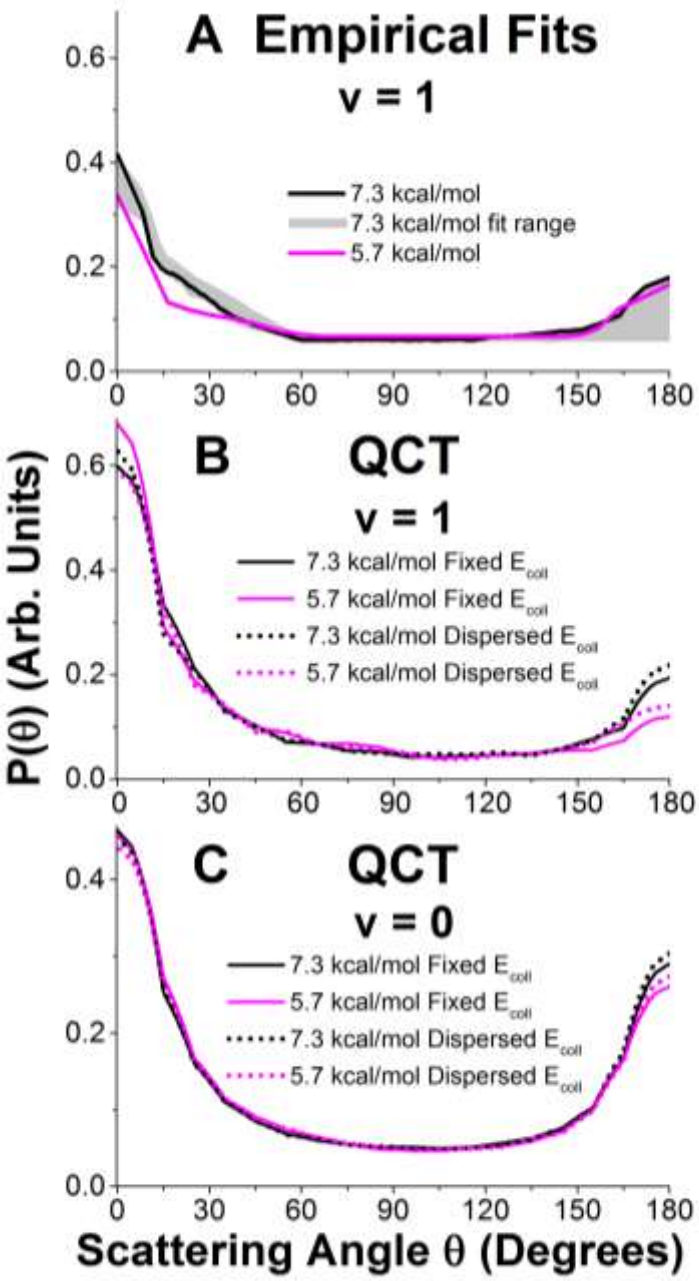

FIG. 10. Comparison of product angular distributions at two different collision energies: P(θ)s are shown for E_{coll} = 7.3 kcal/mol (black lines) and E_{coll} = 5.7 kcal/mol (pink lines) for (A) empirical fits for $^{34}O_2$ in the v = 1 channel (where the gray shaded region is an estimate of the uncertainty in the 7.3 kcal/mol fit from Figure 4); (B) QCT predictions for $^{34}O_2$ in the v = 1 channel with solid lines for fixed E_{coll} and dotted lines for dispersed E_{coll}; and (C) same as (B) for the v = 0 channel.

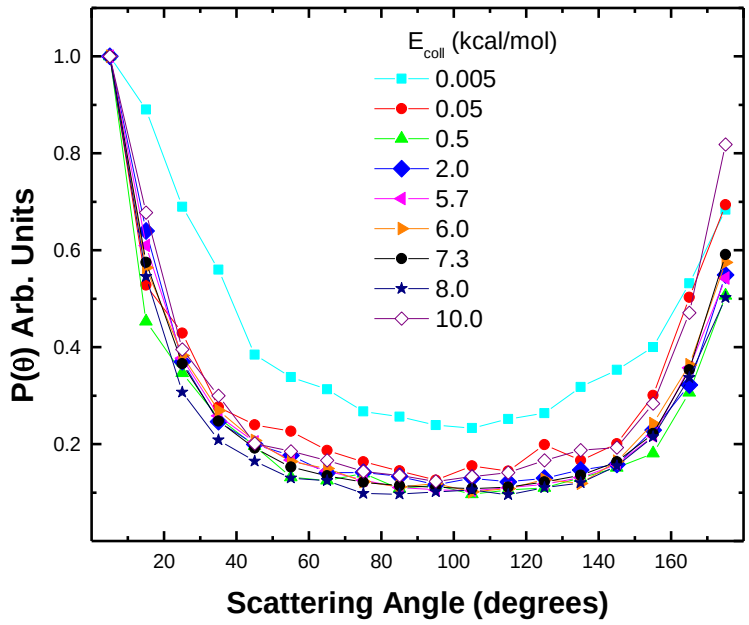

FIG. 11. QCT product angular distributions at various fixed collision energies: All distributions are scaled to one at the forward peak (5°) so that distributions with lower backwards peaks correspond to higher forward bias.

SUPPLEMENTAL MATERIAL

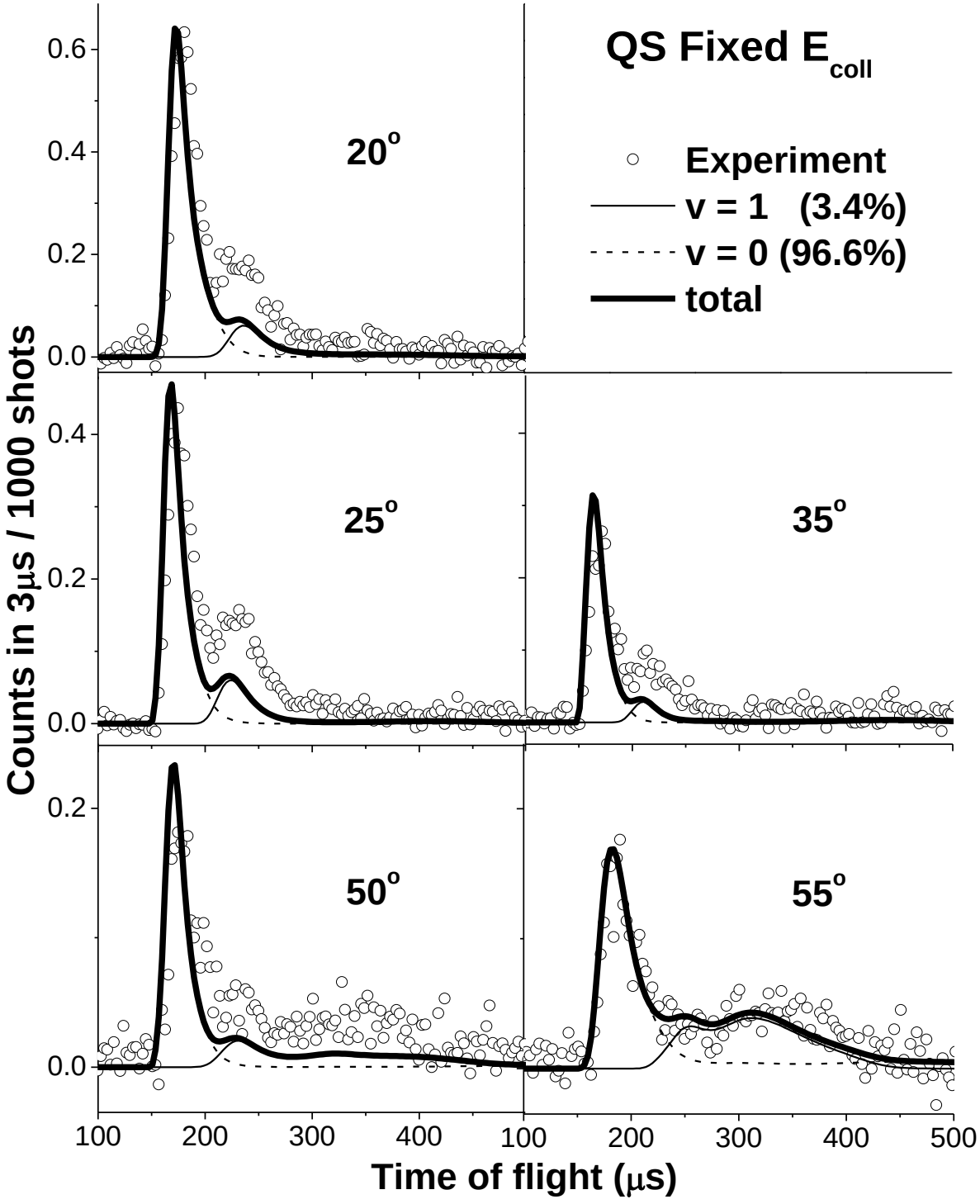

FIG. S1. Time-of-flight spectra for m/z = 34 ($^{18}O^{16}O$) (open circles) **and the QS Fixed E_{coll} prediction** (solid lines) **for E_{coll} = 5.7 kcal/mol.** Note different y-axis scales.

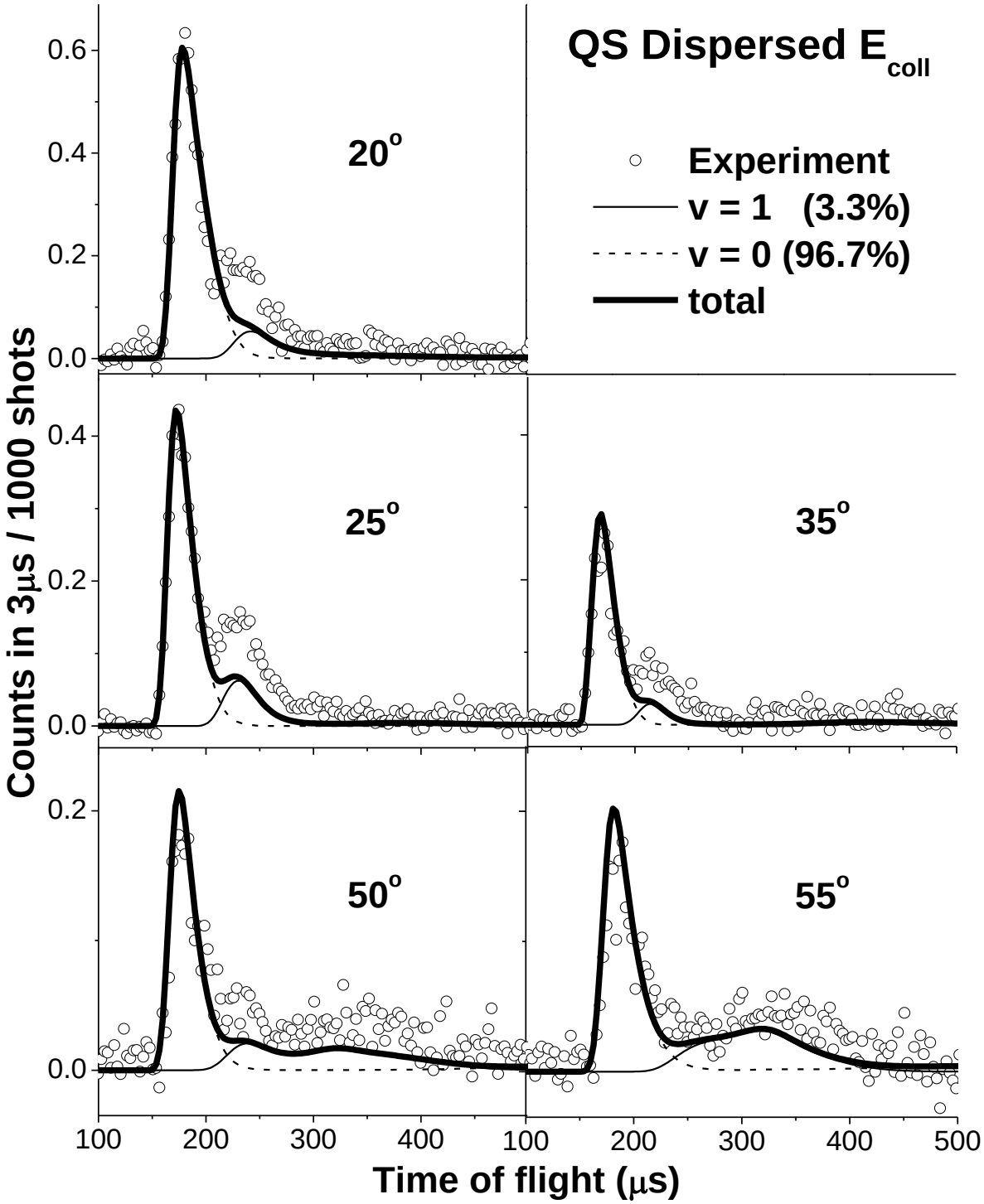

FIG. S2. Time-of-flight spectra for m/z = 34 ($^{18}O^{16}O$) (open circles) **and the QS Dispersed E_{coll} prediction** (solid lines) **for E_{coll} = 5.7 kcal/mol.** Note different y-axis scales.

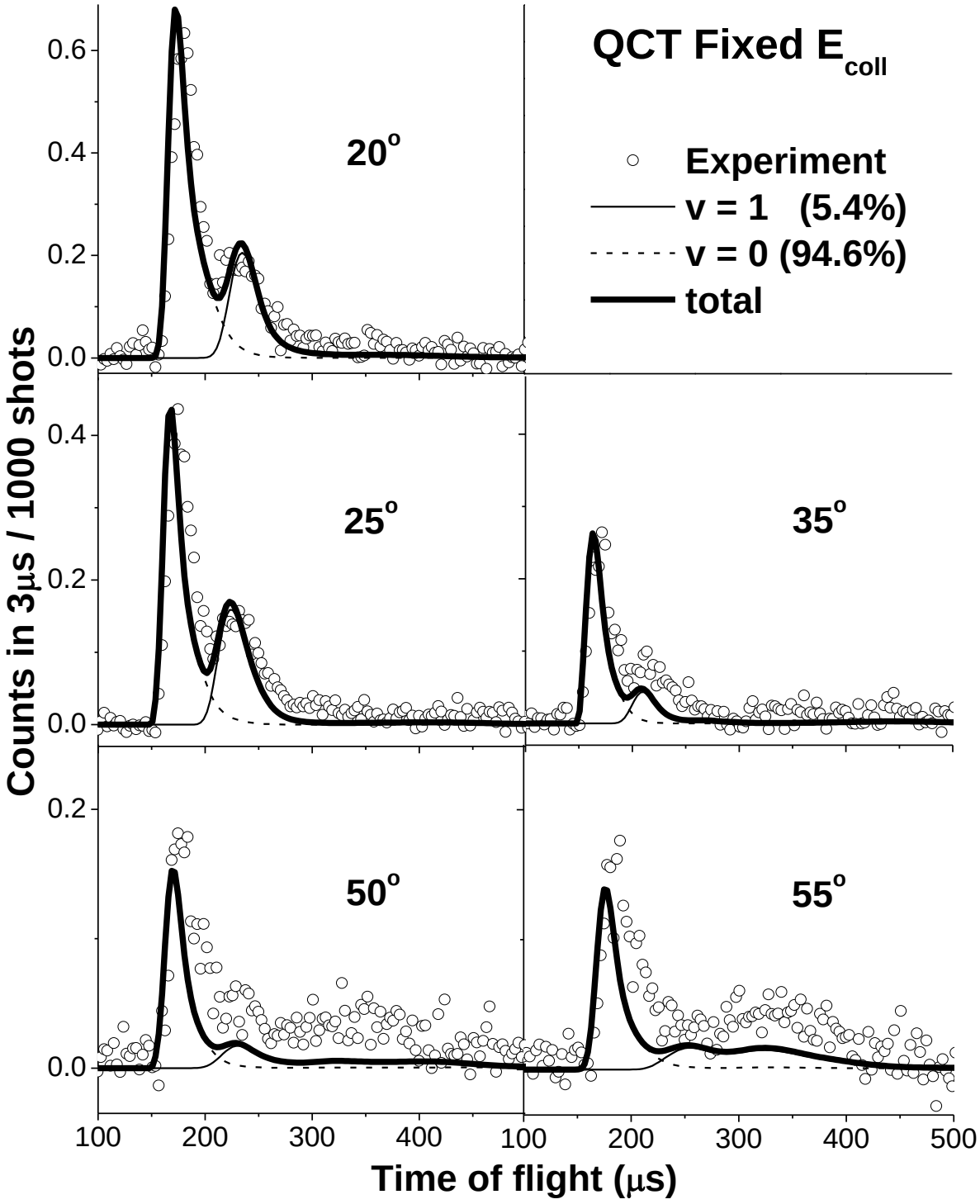

FIG. S3. Time-of-flight spectra for m/z = 34 ($^{18}O^{16}O$) (open circles) **and the QCT Fixed E_{coll} prediction** (solid lines) **for E_{coll} = 5.7 kcal/mol.** Note different y-axis scales.

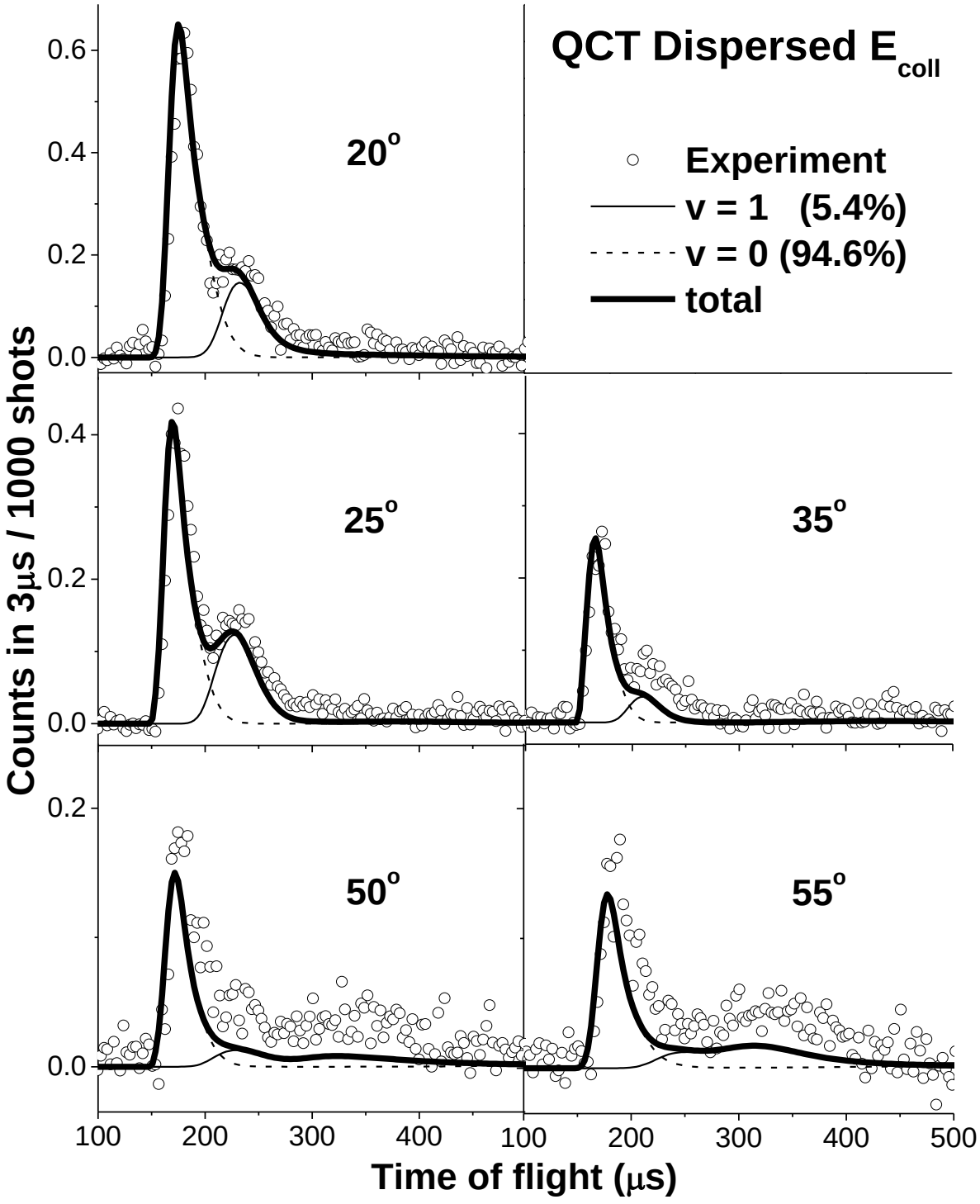

FIG. S4. Time-of-flight spectra for m/z = 34 ($^{18}O^{16}O$) (open circles) **and the QCT Dispersed E_{coll} prediction** (solid lines) **for E_{coll} = 5.7 kcal/mol.** Note different y-axis scales.

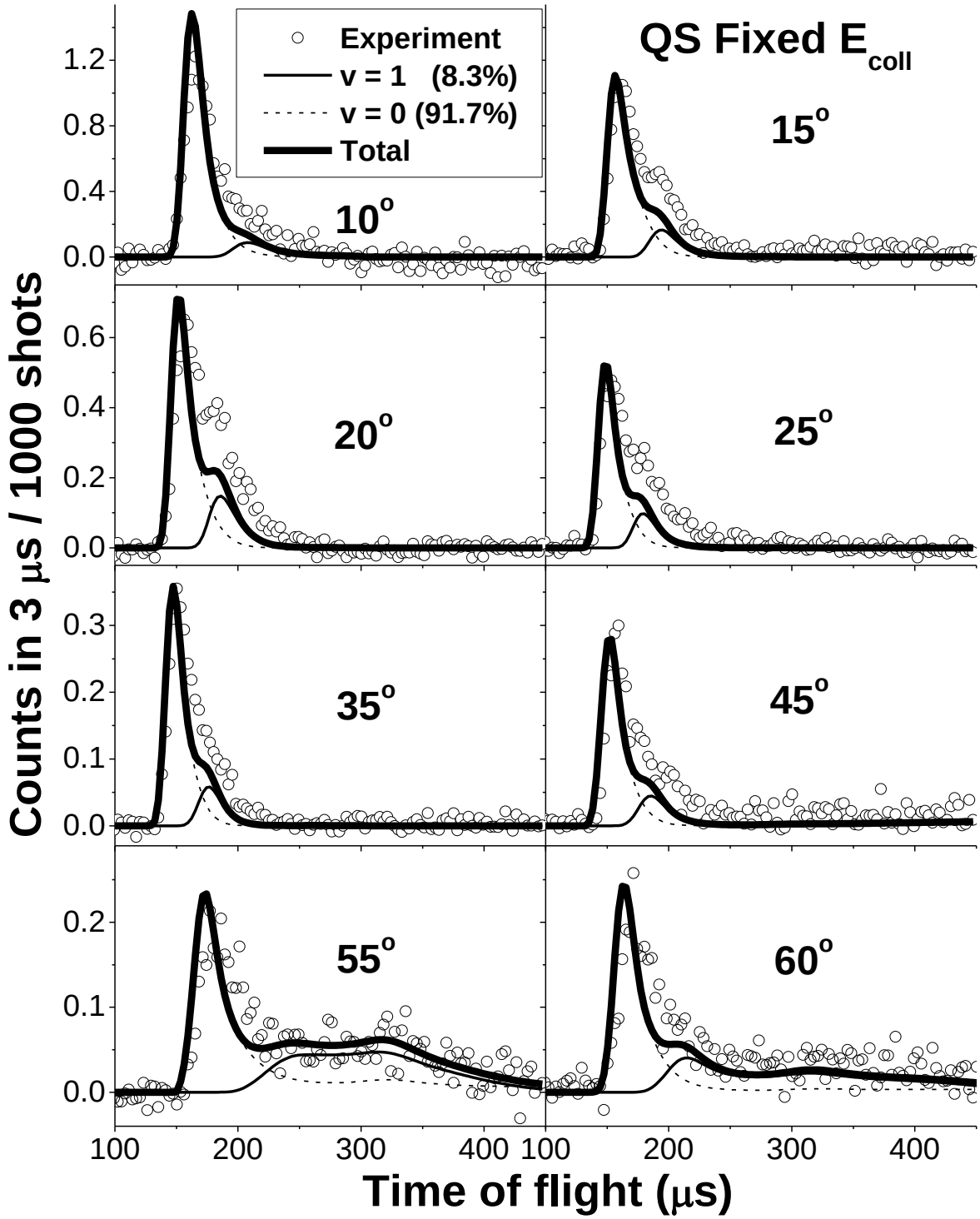

FIG. S5. Time-of-flight spectra for m/z = 34 ($^{18}O^{16}O$) (open circles) **and the QS Fixed E_{coll} prediction** (solid lines) **for E_{coll} = 7.3 kcal/mol.** Note different y-axis scales.

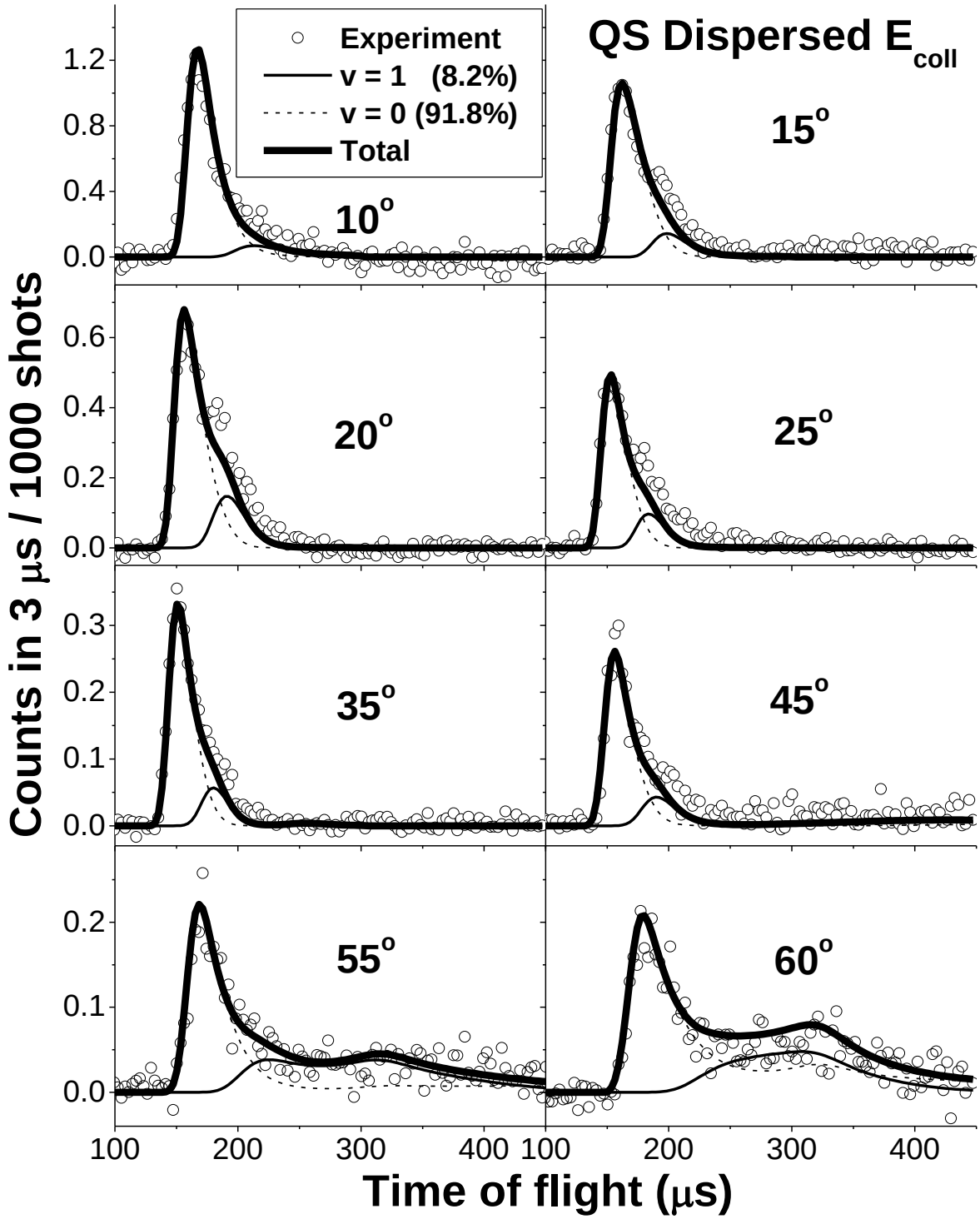

FIG. S6. Time-of-flight spectra for m/z = 34 ($^{18}O^{16}O$) (open circles) **and the QS Dispersed E_{coll} prediction** (solid lines) **for E_{coll} = 7.3 kcal/mol.** Note different y-axis scales.

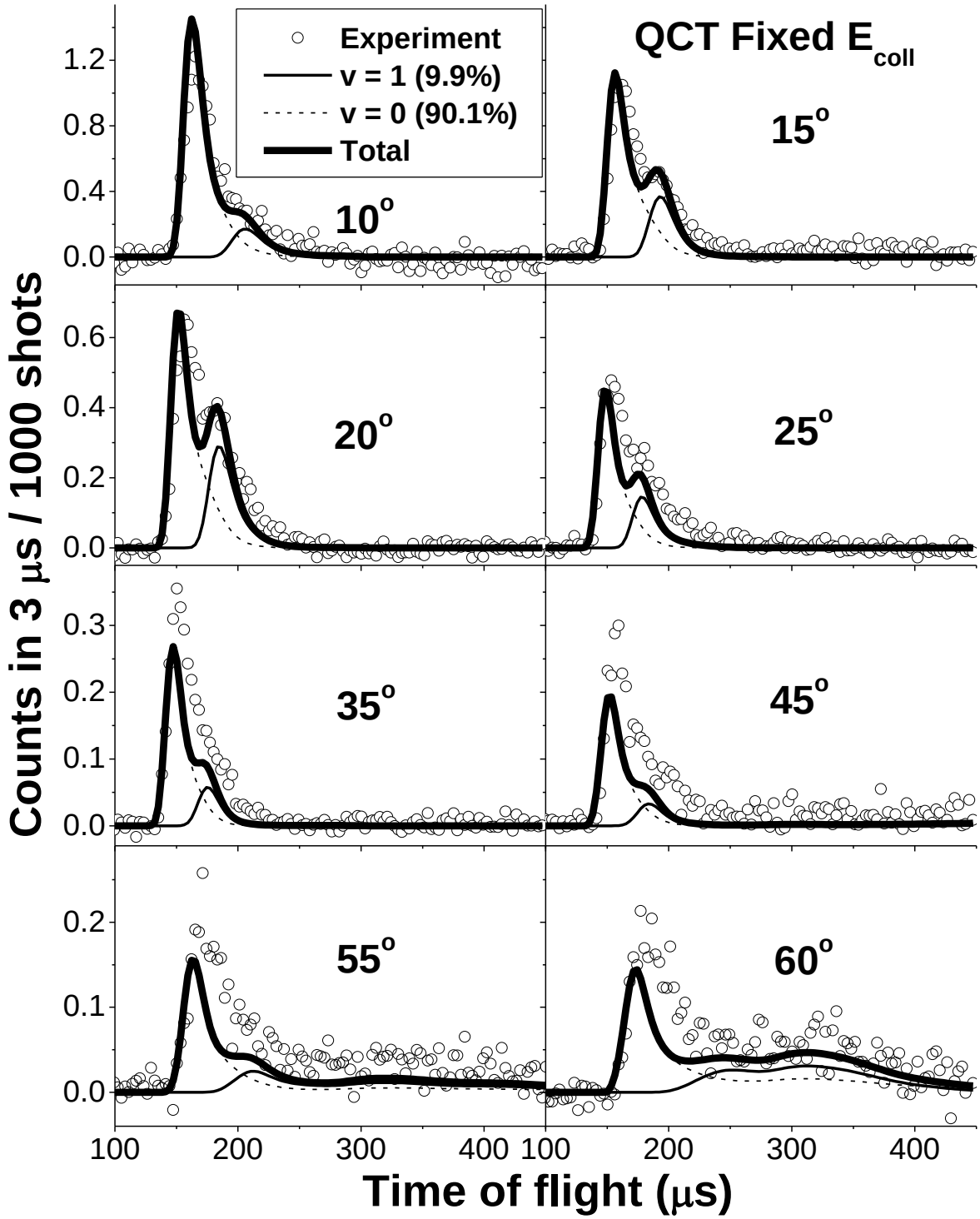

FIG. S7. Time-of-flight spectra for m/z = 34 ($^{18}O^{16}O$) (open circles) **and the QCT Fixed E_{coll} prediction** (solid lines) **for E_{coll} = 7.3 kcal/mol.** Note different y-axis scales.

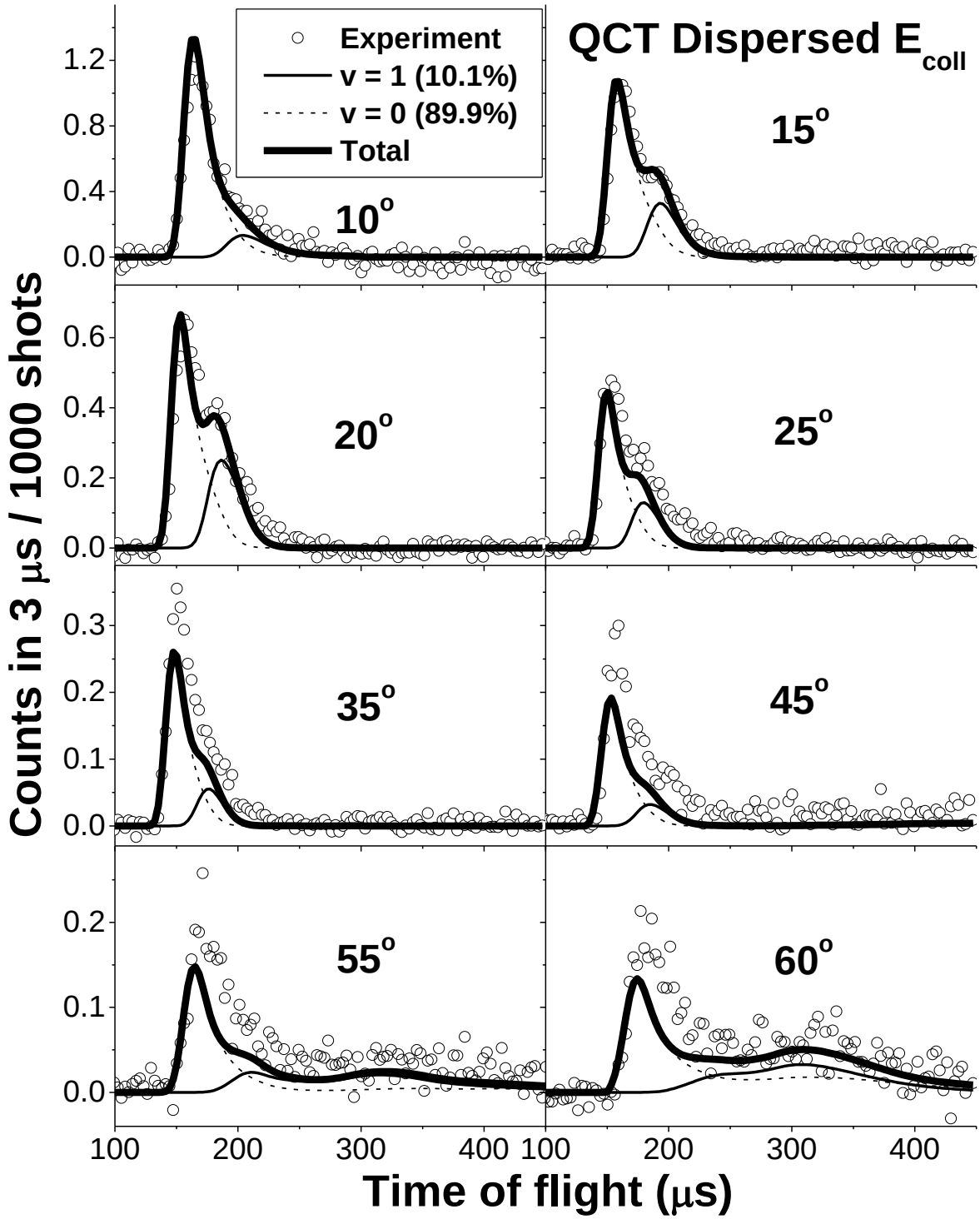

FIG. S8. Time-of-flight spectra for m/z = 34 ($^{18}O^{16}O$) (open circles) **and the QCT Dispersed E_{coll} prediction** (solid lines) **for E_{coll} = 7.3 kcal/mol.** Note different y-axis scales.